Reconstruction of a volcano-sedimentary environment shared by the Porongos and Várzea do Capivarita complexes at 790 Ma, Dom Feliciano Belt, southern Brazil

Matheus Ariel **Battisti**[a], Maria de Fátima **Bitencourt**[a], Renata da Silva **Schmitt**[b], Lauro Valentim Stoll **Nardi**[a], Mariana Maturano Dias **Martil**[a], Giuseppe Betino **De Toni**[a,c], Márcio Martins **Pimentel**[d], Richard **Armstrong**[e], Jiri **Konopásek**[f,g]

a- Programa de Pós-graduação em Geociências, Instituto de Geociências, Universidade Federal do Rio Grande do Sul, Porto Alegre, Brazil

b- Departamento de Geologia – IGEO, Universidade Federal do Rio de Janeiro, Rio de Janeiro, Brazil

c- Universidade Federal Do Pampa (Unipampa), Caçapava do Sul, RS, Brazil

d- Universidade de Brasília, Brasília, Brazil, *in memorian*

e- Research School of Earth Science, Australian National University, ANU, Canberra, Australia

f- Department of Geosciences, UiT–The Arctic University of Norway, Tromsø, Norway

g- Czech Geological Survey, Prague, Czech Republic

Corresponding author: Matheus Ariel Battisti, matheus.ariel.battisti@gmail.com

Address: IGEO – UFRGS, Campus do Vale, Av. Bento Gonçalves, 9500 – Porto Alegre, 91501-970, RS, Brasil.

ABSTRACT

This work investigates the pre-collisional (before ca. 650 Ma) history of the Dom Feliciano Belt in southernmost Brazil through geochronological and zircon oxygen isotope study. U–Pb SHRIMP dating of two orthogneiss samples from the Várzea do Capivarita Complex and one metarhyolite sample from the Porongos Complex yielded crystallisation ages of 786 ± 5 Ma, 780 ± 10 Ma and 787 ± 5 Ma, respectively. The mean oxygen isotope values calculated for the ca. 790 Ma zircon cores from the orthogneisses are 8.41 ± 0.13‰ and 8.68 ± 0.14‰, and 8.75 ± 0.72‰ for the metarhyolite. Such values suggest that zircon crystallised in the more evolved magmas, either from the melting of host rocks and sediments or assimilation of crustal material by mantle-derived magmas. The detrital zircon population was analysed in one additional paragneiss sample from the Várzea do Capivarita Complex, and most of the values cluster at 790–750 Ma. The data spread is centred at ca. 790 Ma, which is the crystallisation age of the interleaved orthogneisses. In our interpretation, such dataset suggests a syn-volcanic origin of the paragneiss protolith and, therefore, a volcano-sedimentary origin of the Várzea do Capivarita Complex. The correspondence of geochronological data and zircon oxygen isotope values for the studied meta-igneous samples suggests that the Várzea do Capivarita and Porongos complexes have shared the same igneous history. Therefore, the samples probably represent one magmatic event at different levels of a single basin at ca. 800-770 Ma. Such results bring first-order information about the meaning of tectonic limits in this Gondwana-related belt and implications for reconstructing the pre- collisional history of the orogen.

Keywords: *Pre-collisional setting, Volcano-sedimentary origin, U-Pb zircon dating, Detrital zircon, Oxygen isotope in zircon*

1. INTRODUCTION

The architecture of pre-collisional scenarios is difficult to reconstruct due to subsequent mountain-building processes (e.g. Cawood et al., 2009; Vanderhaeghe, 2012; Chetty, 2017), including extensive deformation and emplacement of post-orogenic magmatic rocks that mask the former pre-orogenic relations. Thus, pre-orogenic basins commonly have their original stratigraphy completely modified during deformation (Tavani et al., 2015; Lacombe and Bellahsen, 2016), disturbed also by contemporaneous high-grade metamorphism and partial melting (Collins, 2002), and thrusting of the basement (Lacombe and Bellahsen, 2016). Furthermore, in fold-and-thrust belts, as in the case of the Dom Feliciano Belt in South America, thrust sheets and shear zones make the pre-orogenic reconstruction even more difficult, as allochthonous sheets can be carried over thousands of kilometres, often causing an inversion of the original stratigraphy, and high-grade rocks are placed on top of lower grade ones, as observed in the Himalayas, for instance (Harrison et al., 1999). Nevertheless, some approaches can be chosen to address these problems.

This paper aims to reconstruct as far as possible the pre-orogenic scenario of the Central Dom Feliciano Belt, in southeast South America, based on geochronological and oxygen zircon isotope studies in metavolcanic rocks interleaved with metasedimentary sequences. We present new U-Pb and O isotope data on zircons of para- and ortho-derivated rocks from two Tonian metavolcano-sedimentary complexes: Várzea do Capivarita and Porongos. These complexes are now exposed at different levels and have historically been treated as independent units due to their highly contrasting metamorphic grades. Therefore, we have applied an integrated approach to study and compare their common magmatic fraction and discuss their possible paleoenvironments. The results are compared with geochronological and oxygen zircon isotope data reported for these complexes in the literature, and data for the Cerro Olivo Complex (Uruguay), providing new insights into the tectonic evolution of an orogenic belt that runs along southeastern South America and southwestern Africa coasts. Our data provide evidence for a connection between the early Neoproterozoic pre-tectonic processes (at 800-770 Ma) in the hinterland and foreland of the Dom Feliciano Belt in southernmost Brazil, as they developed during the 650 Ma main collisional event.

2. GEOLOGICAL SETTING

2.1 Dom Feliciano–Kaoko–Gariep Orogenic System

The study area is located in the Dom Feliciano Belt (DFB, Fig. 1). The DFB is the South American counterpart of an N-S-trending Neoproterozoic orogenic system that also involves the African Kaoko and Gariep belts. The overall architecture of this orogenic system was developed during the tectonic events between ca. 800 Ma and 550 Ma (Frimmel and Frank, 1998; Oriolo et al., 2017). Some authors interpret the ca. 800 Ma high-grade orthogneisses as related to a continental arc (Koester et al., 2016; Martil et al., 2017; De Toni et al., 2020b) or as generated in a back-arc/rift setting (Konopásek et al., 2018; Will et al., 2019; Hueck et al., 2022). The system evolved into a contractional tectonic regime generating a ca. 650-620 Ma transpressive regime in the Dom Feliciano Belt (e.g. Gross et al., 2006, 2009; Oyhantçabal et al., 2009; Lenz et al., 2011; Martil, 2016; Peel et al., 2018; Will et al., 2019; De Toni et al., 2020a; Percival et al., 2021, 2022). The transpression continued until at least 580–550 Ma, as recorded by ongoing crustal thickening and associated metamorphism in the orogenic system of African and South American sides (Frimmel and Frank, 1998; Goscombe and Gray, 2008; Höfig et al., 2018; Percival et al., 2022). Such convergent period is related to the final amalgamation of the Gondwana supercontinent (e.g. Rapela et al., 2011; Ramos et al., 2017; Oriolo et al., 2017; Schmitt et al., 2018).

The DFB is divided into northern, central, and southern sectors. The central sector (Rio Grande do Sul state) is further divided into Western, Central and Eastern domains (Fragoso-

Cesar et al., 1986; Fernandes et al., 1992; Basei et al., 2000 - Fig. 1). The Western Domain comprises the Pre-Neoproterozoic basement (2.5 to 2.0 Ga - Hartmann et al., 2000) intruded by arc-related rocks of Tonian–Cryogenian ages (the São Gabriel Arc; 750–680 Ma - Nardi and Bitencourt, 2007; Philipp et al., 2016b).

The Central Domain is represented by low- to medium-grade metavolcano-sedimentary rocks (Porongos Complex; Jost and Bitencourt, 1980 - Fig. 1) of Tonian to Ediacaran age (e.g. Saalmann et al., 2011; Pertille et al., 2017; Höfig et al., 2018) with locally exposed Paleoproterozoic basement (Encantadas Complex; 2.26–2.0 Ga – Hartmann et al., 2003; Philipp et al., 2008). The Central and Western Domains are partially covered by late-orogenic, Ediacaran to Ordovician volcano-sedimentary rocks (Paim et al., 2014). Considering the portion of the orogenic belt closer to the relatively undeformed continental interiors as foreland and the internal part of the orogen, closer to the high-grade core, as hinterland (*sensu* Van Der Pluijm and Marshak, 2003), the Central and part of the Western domains of the DFB in southernmost Brazil are interpreted as belonging to the western foreland relative to the main (ca. 650 Ma) collision. Thin-skin tectonics and relatively low geothermal gradient, as discussed by Battisti et al. (2018) and De Toni et al. (2021) are additional evidence for such interpretation.

The Eastern Domain represents the hinterland and features mainly granitic rocks with high-grade host rocks as roof-pendants. These batholiths are interpreted as a post-collisional granitic belt (Bitencourt and Nardi 1993; Bitencourt and Nardi 2000; Philipp and Machado, 2002), whose emplacement was controlled by a lithospheric-scale discontinuity called the Southern Brazilian Shear Belt (SBSB), active between ca. 650 and 580 Ma (Bitencourt and Nardi, 2000; Nardi and Bitencourt, 2007). In Brazil, roof pendants on the Neoproterozoic granitic rocks show at least three distinct ages: Paleoproterozoic (2.2 and 2.0 Ga – Leite et al., 2000; Gregory et al., 2015), Mesoproterozoic (ca. 1.5 Ga – Chemale et al., 2011) and Tonian (ca. 800-770 Ma - Martil et al., 2011, 2017). The latter ones comprise the high-grade metamorphic rocks known as Várzea do Capivarita Complex (VCC) (Fig. 1), which are, according to many authors (e.g. Oyhantçabal et al., 2009; Martil et al., 2017; Konopásek et al., 2018; Hueck et al., 2022), related to the high-grade rocks of the Cerro Olivo Complex (Masquelin et al., 2011) in the Uruguayan part of the DFB hinterland (Fig. 1).

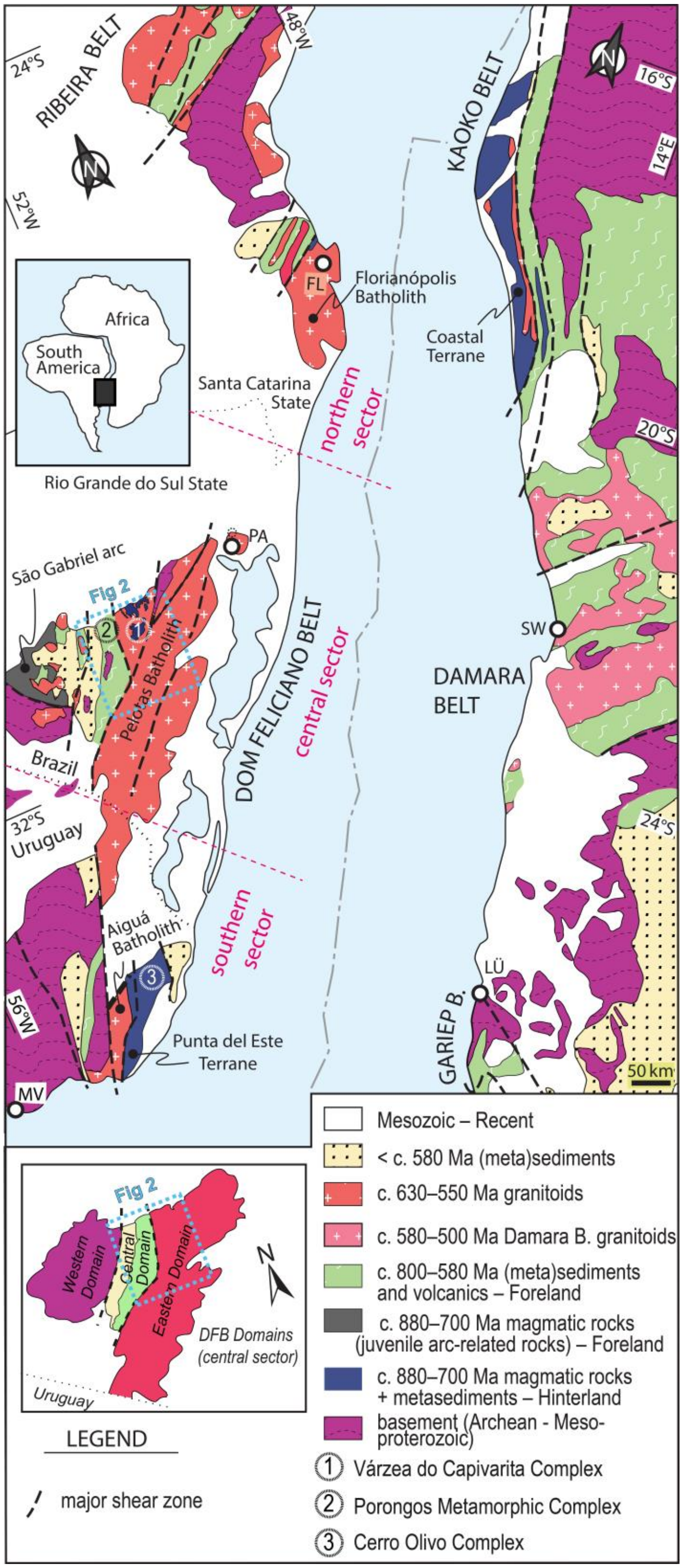

Figure 1. A) Overview geological map and main tectonic domains of the Dom Feliciano–Kaoko–Gariep orogenic system (modified after Bitencourt and Nardi, 2000 and Konopásek et al., 2018). Relative position of Africa and South America is shown at 140 Ma - after Heine et al., 2013. Domains of the Dom Feliciano Belt central sector (Rio Grande do Sul state) and location of figure 2 are indicated in the lower left inset. Cities: FL – Florianópolis, PA – Porto Alegre, MV – Montevideo.

2.2. Tonian metavolcano-sedimentary sequences from DFB

2.2.1. Várzea do Capivarita Complex - *Neoproterozoic high-grade metamorphic rocks in southernmost Brazil*

The Várzea do Capivarita Complex (VCC - Martil et al., 2011, 2017) is part of the Tonian basement intruded by Late Neoproterozoic granites in southernmost Brazil (Fig.1). It is interpreted as a W-verging nappe body thrust onto the Central Domain (Martil et al., 2017; Battisti et al., 2018; De Toni et al., 2021). These well-preserved roof pendants (Martil et al., 2017 - Fig. 2) comprise tectonically interleaved granulite facies orthogneisses and paragneisses (Martil et al., 2011, 2017). According to these authors, the orthogneisses are mostly tonalitic and related to a Tonian mature magmatic arc (790–780 Ma, U–Pb zircon). Paragneisses comprise metapelites and calc-silicate rocks (Martil et al., 2011). The VCC was intruded by syntectonic to post-tectonic plutons from ca. 629 Ma to 578 Ma (e.g. Philipp and Machado, 2002; De Toni et al., 2016; Lyra et al., 2018; Padilha et al., 2019).

The VCC comprises two main deformation phases related to one single tectono-metamorphic event under granulite facies conditions (Gross et al., 2006; Martil, 2016). The VCC gneisses were tectonically interleaved along a subhorizontal banding with top-to-the-west shear sense (Martil et al., 2011; Martil, 2016). Dextral strike-slip to slightly oblique vertical NNE-SSW shear zones progressively overprint the thrust pile (Martil, 2016). PT conditions achieved ca. 750–

800ºC and 3–5 kbar in the VCC metapelites (Gross et al., 2006; Costa et al., 2020; De Toni et al., 2021) at 650–640 Ma (Martil, 2016).

Provenance zircon U-Pb SHRIMP studies of the VCC metasedimentary rocks performed by Gruber et al. (2016a) indicated ages of 2.3 – 2.0 Ga, 1.5 Ga, 1.3 Ga, 930 and 730 Ma for the main source areas, and the maximum deposition age was estimated at 728 ± 11 Ma. According to the same authors, associated marbles were deposited in an interval of ca. 717–750 Ma ($^{87}Sr/^{86}Sr$ initial ratio in whole-rock analyses).

2.2.2. Cerro Olivo Complex - *Neoproterozoic high-grade metamorphic rocks in Uruguay*

In the Uruguayan part of the DFB, crops out the Cerro Olivo Complex (COC - Fig. 1). It is a metaigneous complex with E–W to NW–SE tectonic foliation crosscut by NE-SW strike-slip shear zones (Masquelin et al., 2011). Protolith ages of the COC orthogneisses are reported to be ca. 800-760 Ma (Hartmann et al., 2002; Oyhantçabal et al., 2009; Lenz et al., 2011; Basei et al., 2011; Masquelin et al., 2011; Will et al., 2019). Peak metamorphic conditions were determined at 830–950 ºC and 7–10 kbar (Gross et al., 2009), dated at ca. 650 Ma (Gross et al., 2009; Oyhantçabal et al., 2009; Lenz et al., 2011; Basei et al., 2011; Peel et al., 2018; Will et al., 2019) and this metamorphic event is interpreted as related to the assembly of the Gondwana supercontinent.

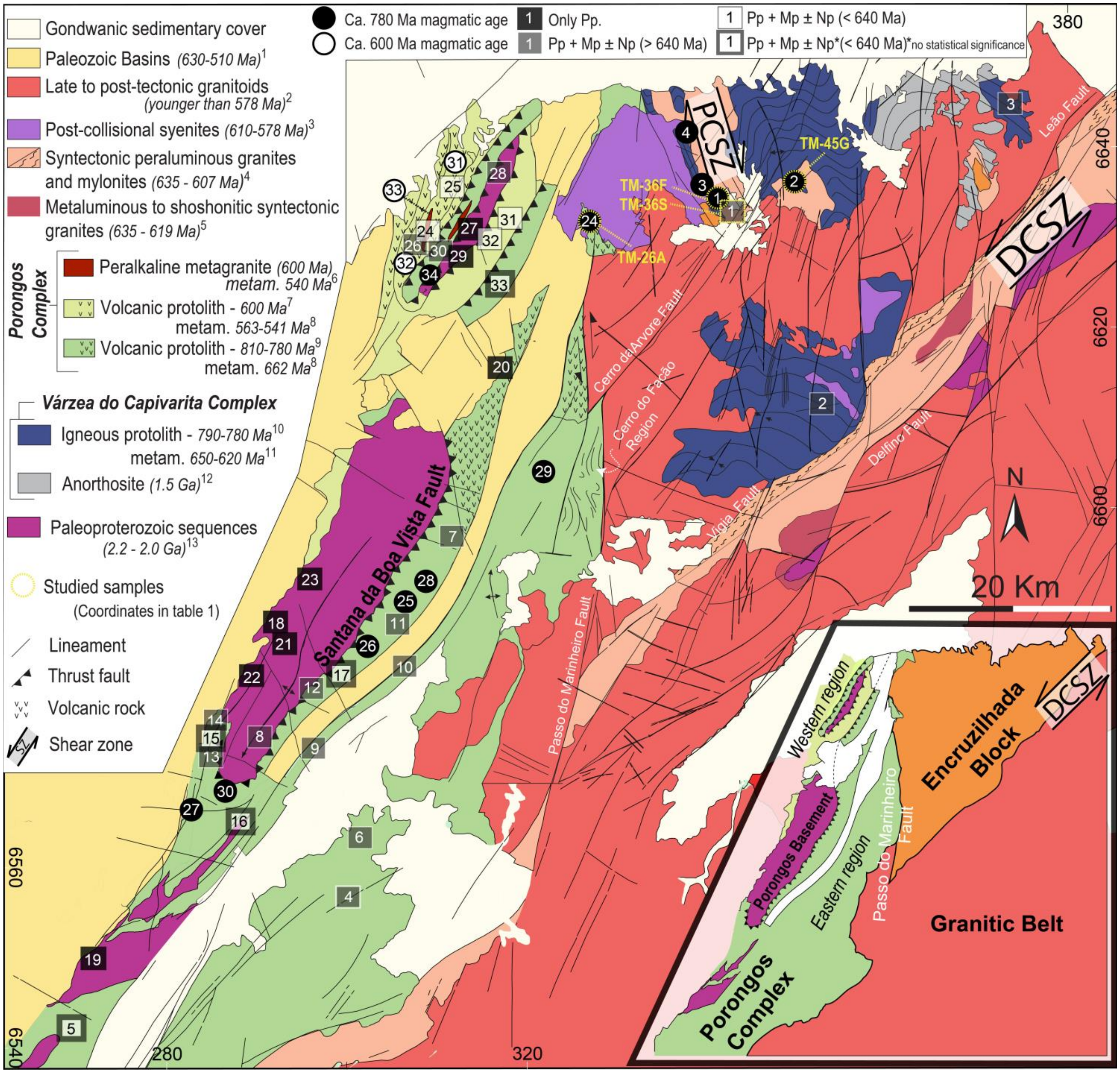

Figure 2. Geological map of the study area with sample sites indicated. Tectonic compartments shown in the inset (after De Toni et al., 2021). Porongos Complex is divided into eastern and western regions (inset) separated by the Santana da Boa Vista fault. Such names do not represent any stratigraphic proposal and should be used only as geographical references They are used in this paper to guide the reader through our discussion. Sample sites from tables 2 and 3 are indicated, in which circles are magmatic ages, while squares represent provenance source ages. Abbreviations: Pp – Paleoproterozoic, Mp – Mesoproterozoic, Np – Neoproterozoic. DCZS – Dorsal de Canguçu Shear

Zone; PCSZ – Passo das Canas Shear Zone. Please note the similar magmatic and provenance ages between VCC and eastern PC and the difference between the magmatic and provenance ages between the PC eastern and western regions - separated by the Santana da Boa Vista thrust fault – References: 1-Paim et al. (2014); 2-Padilha et al. (2019); 3-Rivera (2019); Padilha et al. (2019); 4-Bitencourt et al. (2015); Knijnik (2018); Vieira et al. (2020); 5-Knijnik (2018); Vieira et al. (2020); 6-Philipp et al. (2016b); 7-Höfig et al. (2018); 8-Battisti (2022); 9-Saalmann et al. (2011); Pertille et al. (2017); 10-Martil et al.((2017); 11-Gross et al. (2006); Chemale et al. (2011); Philipp et al. (2016a); Martil et al. (2017); 12-Chemale et al. (2011); 13-Leite et al. (2000); Hartmann et al. (2003); Saalmann et al. (2011); Gregory et al. (2015).

2.2.3. *Porongos Complex* – *Neoproterozoic low- to medium-grade metamorphic unit in Southernmost Brazil*

The Porongos Complex (PC; Jost and Bitencourt, 1980) is interpreted as part of the Dom Feliciano Belt western foreland and comprises Neoproterozoic supracrustal rocks metamorphosed at lower greenschist to middle amphibolite facies (Fig. 1 and 2). The PC comprises metasedimentary and metavolcanic rocks, some ultramafic lenses and, less often, deformed granitoids (Jost and Bitencourt, 1980; Marques et al., 2003; Zvirtes et al., 2017). The PC metamorphic grade increases from west to east, and staurolite-bearing metapelites at the PC easternmost border (Fig. 2) record the highest metamorphic grade of the complex (Jost and Bitencourt, 1980; Lenz, 2006). The PT conditions were estimated at 560–580°C and 5.8–6.3 kbar by De Toni et al. (2021), and the metamorphism was dated at 658 ± 26 Ma (Lenz, 2006; Rb–Sr in muscovite and whole-rock).

Provenance studies in the PC have shown two distinct sources for the metamorphosed clastic sediments (Gruber et al., 2011; Pertille et al., 2015a, 2015b, 2017; Höfig et al., 2018). Based on this difference, Höfig et al. (2018) suggested that the precursor of the Porongos

Complex could have been two distinct and diachronous basins. The older PC metasedimentary rocks (mostly at its eastern part – Fig. 2) represent mostly clastic infill of a pre-orogenic basin with dominant Paleoproterozoic (2.0–2.3 Ga), subordinate Mesoproterozoic (1.2–1.5 Ga) and rare ca. 750-800 Ma detrital sources (provenance interval: 750 Ma to 3.0 Ga - Gruber et al., 2016b; Pertille et al., 2017; Höfig et al., 2018). The younger PC basin presents metasedimentary rocks related to the syn-orogenic (from ca. 650 Ma onwards) evolution, as discussed by Höfig et al. (2018) and Battisti et al. (2018). In the western part of the PC (Fig. 2), the syn-orogenic metasedimentary rocks are interleaved with the rocks of the older basin. Their detrital zircon populations show mainly Paleoproterozoic (2.0–2.3 Ga) and Neoproterozoic (ca 600 and ca 800 Ma) sources (provenance interval: 570 Ma to 3.2 Ga - Pertille et al., 2015b, 2017; Gruber et al., 2016b; Höfig et al., 2018). Associated intermediate to acid metavolcanic rocks also yielded contrasting ages in different regions of the complex. The PC eastern region contains metavolcanic rocks with protolith ages of ca. 800–770 Ma (Saalmann et al., 2011; Pertille et al., 2017), whereas magmatic ages of 600 and 601 Ma were obtained for metavolcano-sedimentary rocks of the PC western region (LA–MC–ICP–MS U–Pb zircon - Höfig et al., 2018). Such dataset shows that the igneous activity and late sedimentation in the western PC is younger than the metamorphic peak recorded in its eastern portion (658 ± 26 Ma - Lenz, 2006). The so-called Eastern and Western Porongos Complex regions are distinguished based on their position relative to the main W-verging thrust fault, the Santana da Boa Vista Thrust Fault, as originally defined by Jost and Bitencourt (1981 – fig. 2).

3. PETROGRAPHY

Four representative samples were selected considering previous detailed field studies (location in Fig. 2). Three samples represent the lithological variations of the Várzea do Capivarita Complex. They include orthogneisses of tonalitic (TM-36F) and granitic composition (TM-45G), and an aluminous paragneiss (TM-36S), all metamorphosed under granulite facies conditions. The tonalitic orthogneiss and the aluminous paragneiss are interleaved along a flat-lying foliation related to the main deformation phase (Martil, 2016). The granitic orthogneiss sample has a subvertical fabric in high-strain zones that overprint the flat foliation. Finally, a sample of metavolcanic rock (TM-26A) with geochemical features and structural evolution similar to the VCC samples (Martil, 2016; Martil et al., 2017; Battisti et al., 2018) was collected in the eastern portion of the Porongos Complex, at the contact of the Central and Eastern domains (Fig. 1 and 2). Outcrop features of the investigated samples are shown in figure 3.

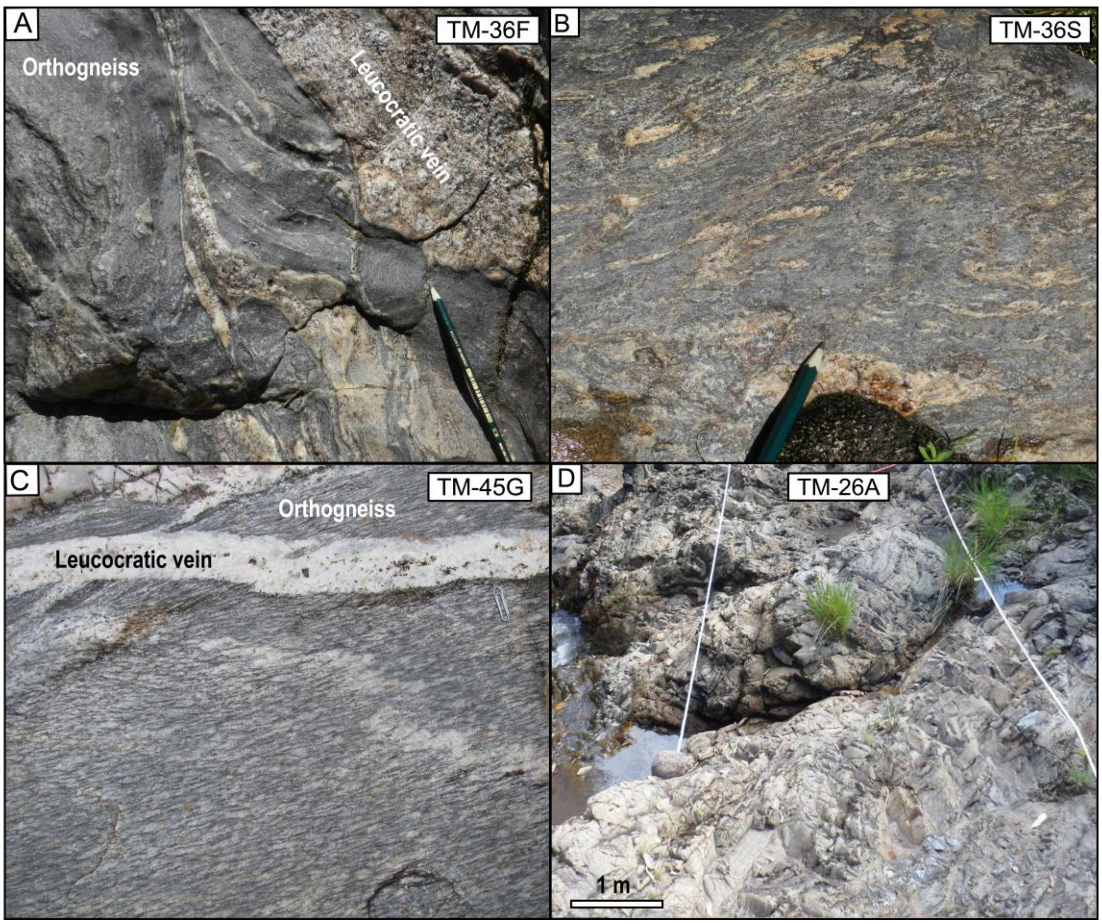

Figure 3. A) Fine-grained TM-36F orthogneiss. B) Outcrop of the sampled paragneiss TM-36S with local veins resulting from partial melting. C) TM-45G granitic orthogneiss. D) Outcrop view of the metarhyolite TM-26 A.

Sample TM-36F is a poorly-banded, fine- to medium-grained orthopyroxene-bearing hornblende-biotite tonalitic orthogneiss with granolepidoblastic seriate–interlobate texture (Fig. 4a, b). Rounded plagioclase megacrysts and rare K-feldspar are ca. 1 mm-large but can reach up to 3 mm. They are set in a fine-grained (0.3 mm) matrix containing plagioclase, K-feldspar, quartz and biotite (Fig. 4b). Biotite is subhedral and forms discontinuous bands. Remnant orthopyroxene is locally preserved in pseudomorphic clusters, in which hornblende crystals up to 0.5 mm long with nematoblastic to decussate texture and biotite crystals have grown. Opaque minerals, zircon and secondary chlorite are also present.

Sample TM-36S is an irregularly banded, dark-grey coloured, spinel-sillimanite-bearing garnet-cordierite-biotite paragneiss from the same outcrop as the previous sample (Fig. 3). Mafic-rich bands are up to several cm thick and alternate with felsic bands/lenses of millimetre thicknesses (Fig. 4c). Biotite is the main mafic mineral, displaying continuous bands with 0.3 and 0.5 mm-size subhedral crystals. Felsic bands are composed of 0.5 to 1 mm large quartz, subordinate plagioclase and rare K-feldspar, all of which exhibit granoblastic interlobate to granoblastic polygonal texture (Fig. 4d). Garnet and cordierite are present in both mafic- and felsic-rich layers. Garnet is subhedral (0.5 to 1 mm), poikiloblastic and includes numerous quartz crystals. Cordierite is commonly transformed into pinnite. Rare dark-green chromium-rich spinel is preserved as inclusions in cordierite. The rock contains rare tiny prismatic sillimanite crystals (0.1 mm), apatite and zircon. The interpretation of sample TM-36S as a paragneiss is based on the following criteria: i) At the same outcrop, TM-36S is interleaved with calc-silicate layers, while in TM-36F tonalitic orthogneiss bands, calc-silicate layers are absent; and ii) The amount of quartz is larger than the feldspar content in TM-36S, which is not expected for a granitic origin.

Sample TM-45G is a granolepidoblastic, well-foliated garnet-biotite granitic orthogneiss (Fig. 4e, f) of medium-grained equigranular texture. Plagioclase, K-feldspar and quartz exhibit high-temperature recrystallisation features. Biotite crystals are 1 to 2 mm long and occur in mm-thick, mica-rich layers. Garnet is an accessory mineral with 0.2 to 0.5 mm.

TM-26A is a PC blastoporphyritic metarhyolite with ca. 3 mm-long aggregates of blue quartz (Fig. 4g, h) set in a very fine-grained (0.01 mm) granolepidoblastic matrix composed of quartz, feldspar and greenish biotite (Fig. 4h). Millimetre-sized quartz aggregates are often stretched, and quartz crystals are either partially or completely recrystallised to granoblastic texture with interlobate contacts. Larger brown biotite crystals (0.2 mm) display poorly-developed, mm-thick layers. Accessory minerals are opaque minerals (mainly ilmenite), apatite and zircon.

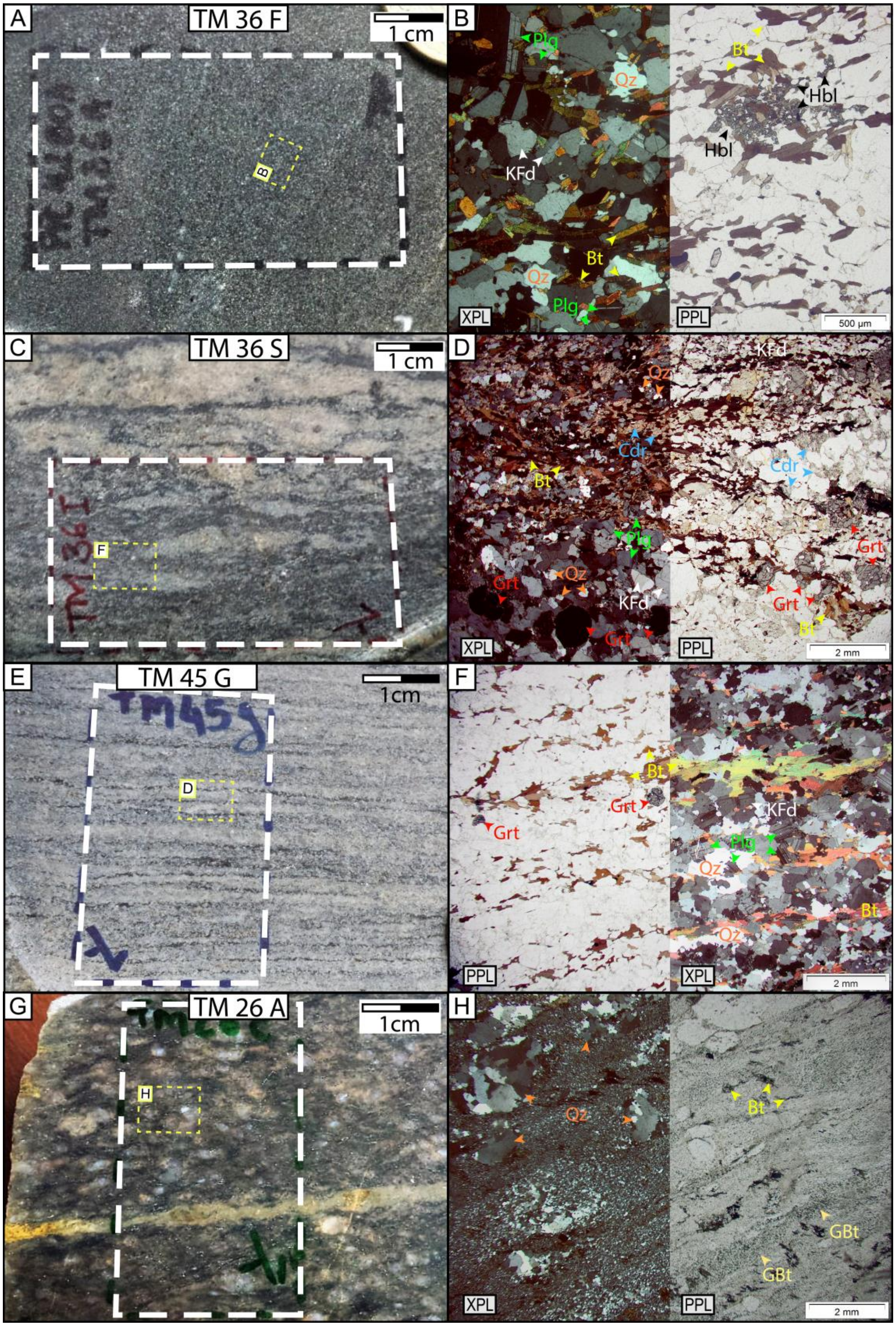

Figure 4. The four studied samples (location in Fig. 2). TM-36F - Várzea do Capivarita Complex tonalitic orthogneiss - A) and B); TM-36S - Várzea do Capivarita Complex paragneiss - C) and D); TM-45G - Várzea do Capivarita Complex granitic orthogneiss - E) and F); TM-26A - Porongos Complex eastern

region blastoporphyritic metarhyolite - G) and H). Thin-section locations and pictures of detailed areas are indicated. Note that photomicrographs at the right were taken in both plane-polarized (PPL) and cross-polarised light (XPL) to highlight textural aspects of the rock. Mineral abbreviations: Qz – quartz, Plg – Plagioclase, KFd – K-feldspar, Bt – biotite, GBt– green biotite, Hbl – hornblende, Grt – garnet, Cdr – cordierite.

4. ANALYTICAL TECHNIQUES

The samples were crushed, and the zircons were separated using standard magnetic and heavy liquid density separation techniques. The clean zircon separates were mounted in epoxy at the Research School of Earth Sciences (RSES), Australian National University, together with the RSES reference zircon AS3 and SL13. Zircon grains were handpicked under a binocular microscope or, in the case of the detrital zircons, scattered onto double-sided tape before mounting in epoxy to ensure a random selection of grains.

Photomicrographs of all zircons were taken in transmitted and reflected light. Together with SEM cathodoluminescence (CL) images, these were used to decipher the sectioned grains' internal structures and select specific areas within the zircons for spot analysis. U–Pb analysis was carried out using SHRIMP I, SHRIMP II and SHRIMP RG at the RSES. The data were reduced in a manner similar to that described by Williams (1998 and references therein), using the SQUID-1 Excel Macro of Ludwig (2003). For the zircon calibration, the Pb/U ratios were normalised relative to a value of 0.1859 for the $^{206*}Pb/^{238}U$ ratio of AS3 reference zircons, equivalent to an age of 1099 Ma (Paces and Miller, 1993). U and Th concentrations were determined relative to the SL13 standard. Common Pb was corrected using measured ^{204}Pb. Uncertainties given for single analyses (ratios and ages) are at the 1σ level, but uncertainties in any calculated weighted mean, concordia age (Paces and Miller, 1993), or intercept age are reported as 95% confidence limits (unless indicated otherwise) and include the uncertainties in the standard calibrations where appropriate. Concordia plots, regressions and age calculations were carried out using Isoplot/Ex and SQUID-1 (Ludwig, 2003). Zircon oxygen isotopic data were analysed by SHRIMP SI and, when possible, spots were made directly below to the polished locations of ages measurements. All $\delta^{18}O$ data were normalised to a TEMORA II value of 8.2‰. Complete data of analysed zircons from each sample are presented as supplementary data.

5. U-Pb RESULTS IN ZIRCON

5.1. Orthogneisses (TM-36F and TM-45G)

Samples TM-36F and TM-45G were analysed to determine the crystallisation age of the VCC tonalitic and granitic composition protolith, respectively. In TM-36F, the zircon population is rather homogeneous, and the grains are euhedral to subhedral with shapes ranging from square and almost equidimensional to more elongate prismatic forms (Fig. 5a). CL imaging reveals that internal structures are dominated by sectors with oscillatory zoning of variable intensity. Crystal sizes are ca. 100–250 µm. Some crystals show a core with no zoning, which grades into the oscillatory-zoned rims, the latter showing the most concordant analyses (Fig. 6a). Seventeen spot analyses in the oscillatory zoned domains yielded a concordia age of 786 ± 5 Ma (95% confidence), which is considered the best estimate for the crystallisation age of the igneous protolith (Fig. 6b). Th/U ratios determined for the concordant spots range between 0.28 and 0.68. One crystal (#14.1) without oscillatory zoning and a Th/U ratio of 0.84 gave a Mesoproterozoic concordant age of 1127 ± 15 Ma (Fig. 5a, 6a), interpreted here as an inherited grain. Another crystal displays a $^{206}Pb/^{238}U$ age of 625± 6 Ma (#15.1 – Fig. 5a, 6a); it is smaller than the overall grain size and has a lower Th/U ratio of 0.12.

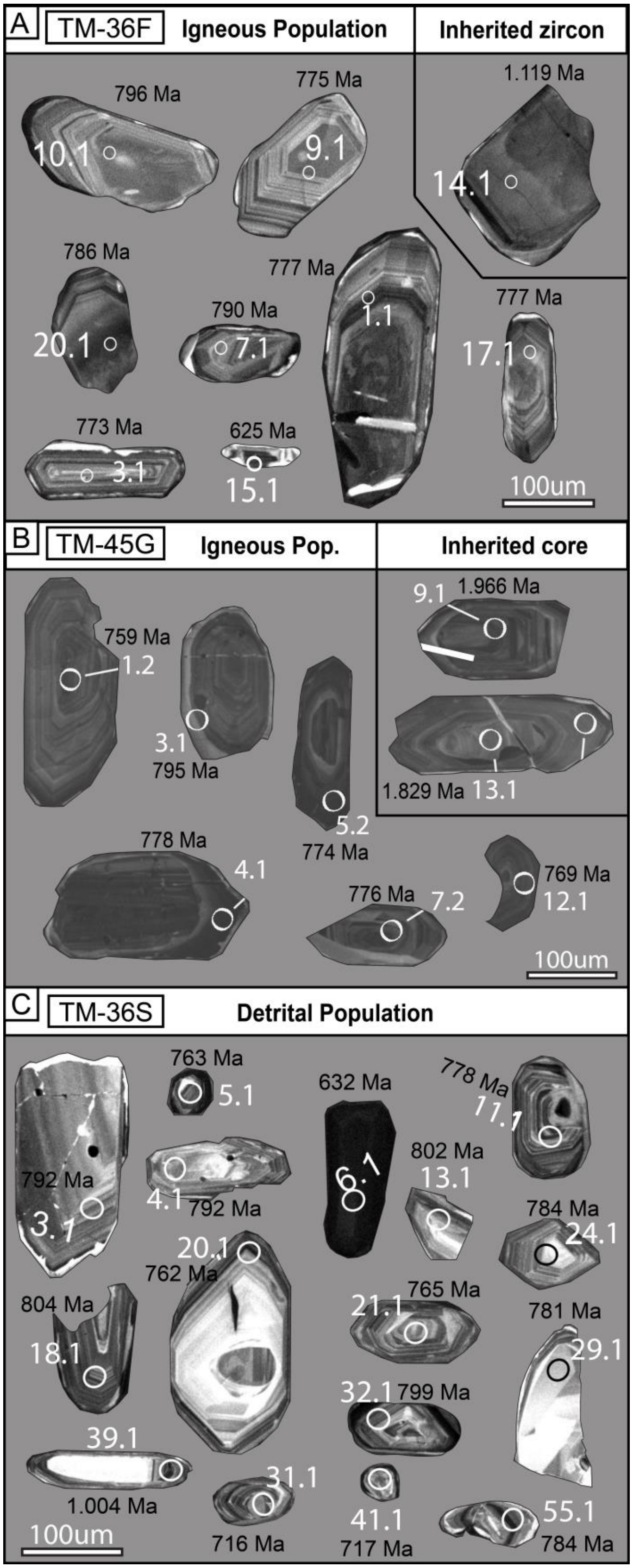

Figure 5. A) Cathodoluminescence images from some zircon crystals of sample TM-36F. Note the bright, thin metamorphic rim on crystals #3.1, #7.1, #17.1, and dark, thin metamorphic rims on crystals #9.1 and #10.1. One crystal (#14.1) without oscillatory zoning gives a Mesoproterozoic concordant age

(Fig. 6A). B) Examples of CL images of zircon crystals from sample TM-45G. Inherited cores are found in spots #9.1 and #13.1. c) Cathodoluminescence images from some detrital zircons of sample TM-36S. Note the youngest analysed zircons (#31.1 and #41.1) at the bottom of the figure. Ages are given as $^{206}Pb/^{238}U$ – complete information is available as supplementary data.

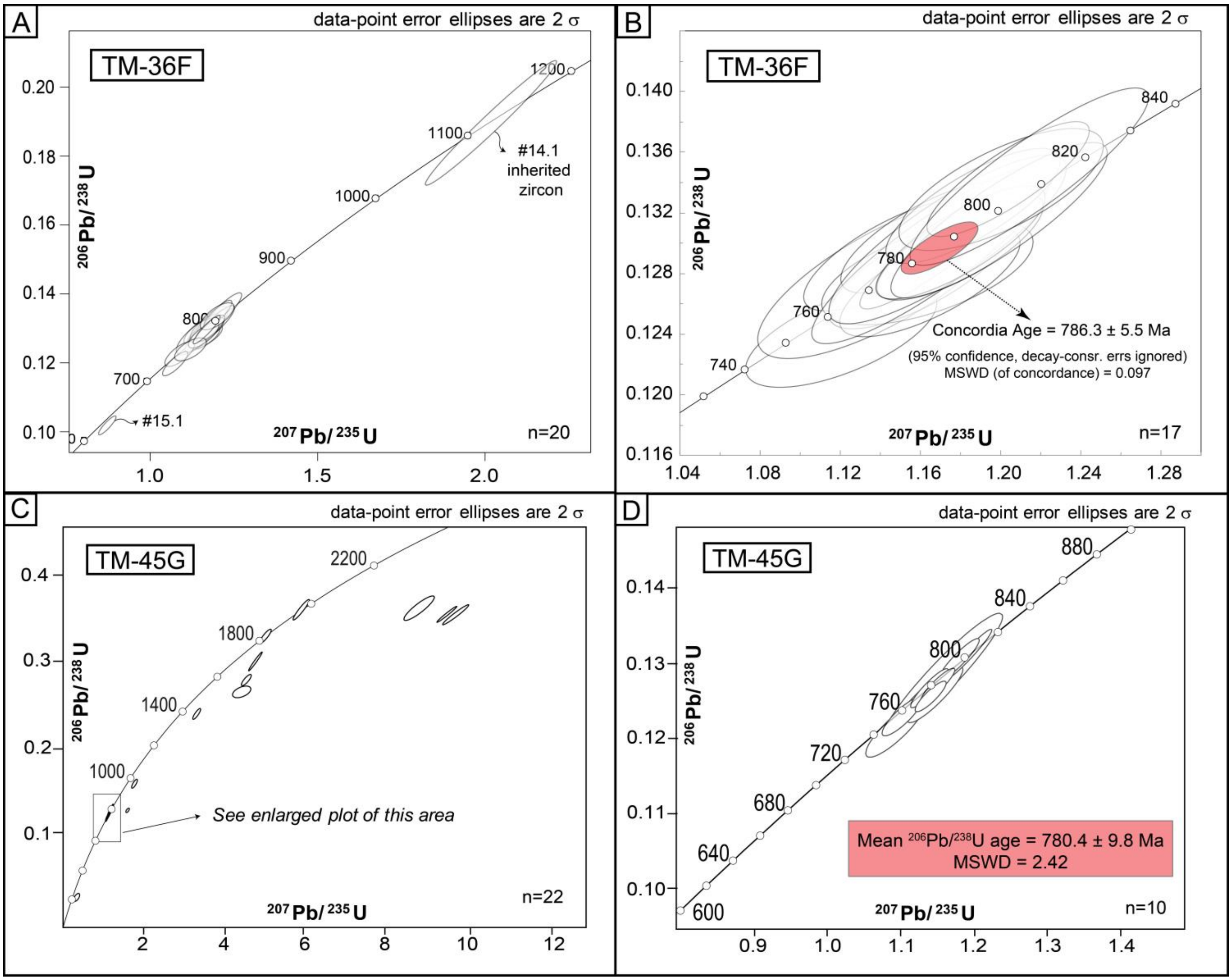

Figure 6. A) Concordia U-Pb diagram with all analysed zircons from tonalitic orthogneiss sample TM-36F; B) U-Pb concordant age is interpreted as the best age for the crystallisation of the protolith of TM-36F; C) Concordia U-Pb diagram with all analysed zircons from granitic orthogneiss sample TM-45G; D) Concordant Neoproterozoic zircons used to calculate the mean $^{206}Pb/^{238}U$, interpreted as the crystallisation age of TM-45G protolith.

Zircon population from sample TM-45G is rather homogeneous and shows euhedral to subhedral, mainly elongate prismatic crystals smaller than 200 µm. Their CL images show typical igneous oscillatory zoning (Fig. 5b). Some crystals present an inner part with no zoning and a light grey area at the rims. Most zircon crystals have a very thin, CL-bright rim, which probably indicates a metamorphic overgrowth; however, the rims are too thin for analysis. Twenty-two SHRIMP analyses were performed in ten different zircon grains, and ten analyses, with Th/U ratios between 0.16 and 0.54 yielded a mean $^{206}Pb/^{238}U$ age of 780 ± 10 Ma (MSWD = 2.42), which is interpreted as the age of the orthogneiss protolith (Fig 6c,d). Two spots yielded concordant dates at ca. 1.8 and 2.0 Ga, and these are interpreted as inherited grains. Other older grains were dated but had discordant ages (Fig. 6c).

5.2. Paragneiss (TM-36S)

To constrain the maximum age of sedimentation for the VCC, 65 zircon grains were analysed from the paragneiss sample TM-36S. The CL images show typical igneous oscillatory zoning, and the crystal sizes are between 50 and 200 µm. Most crystals are prismatic, euhedral to sub-euhedral (Fig. 5c) with no sign of abrasion, and their sharp pyramidal tips are preserved. Thin CL-bright overgrowths are rare and too thin to be analysed.

The data is shown in two separate concordia diagrams and one relative probability plot (Fig. 7). Considering only the concordant (>95%) analyses, detrital zircon grains from sample TM-36S provided two populations: a minor one at ca. 1.1 Ga, and a more significant at ca. 790 Ma (Fig. 7a, b). Some discordant grains suggest older sources (Fig. 7a).

The 790-750 Ma age interval indicates a major source for the deposition of these para-derived protoliths (Fig. 7c). The analysed grains show Th/U ratios between 0.18 and 0.70, although spot #23.1 has a Th/U ratio of 0.08. The data spread is centred at ca. 790 Ma, which also corresponds to the crystallisation age of the tonalitic orthogneiss TM-36F, as shown by curves of relative probability (Fig. 7c). This would suggest that they are coeval or that the sedimentary protolith of sample TM-36S is mostly a product of erosion of the 790 Ma tonalite/dacite. The predominantly euhedral detrital zircons with well-preserved prismatic tips indicate a short sedimentary transport (near to source). The two youngest detrital zircons constrain the maximum age of sedimentation at 716 Ma (spots #31.1 and #41.1 - at the bottom of Fig 5c).

One crystal reveals a much younger age of 632± 9 Ma (spot #6.1 – Fig. 5c, 8b). It is interpreted as related to the metamorphic granulite facies event because it is morphologically distinct from the others with a homogenous black domain and has Th/U ratio of 0.01.

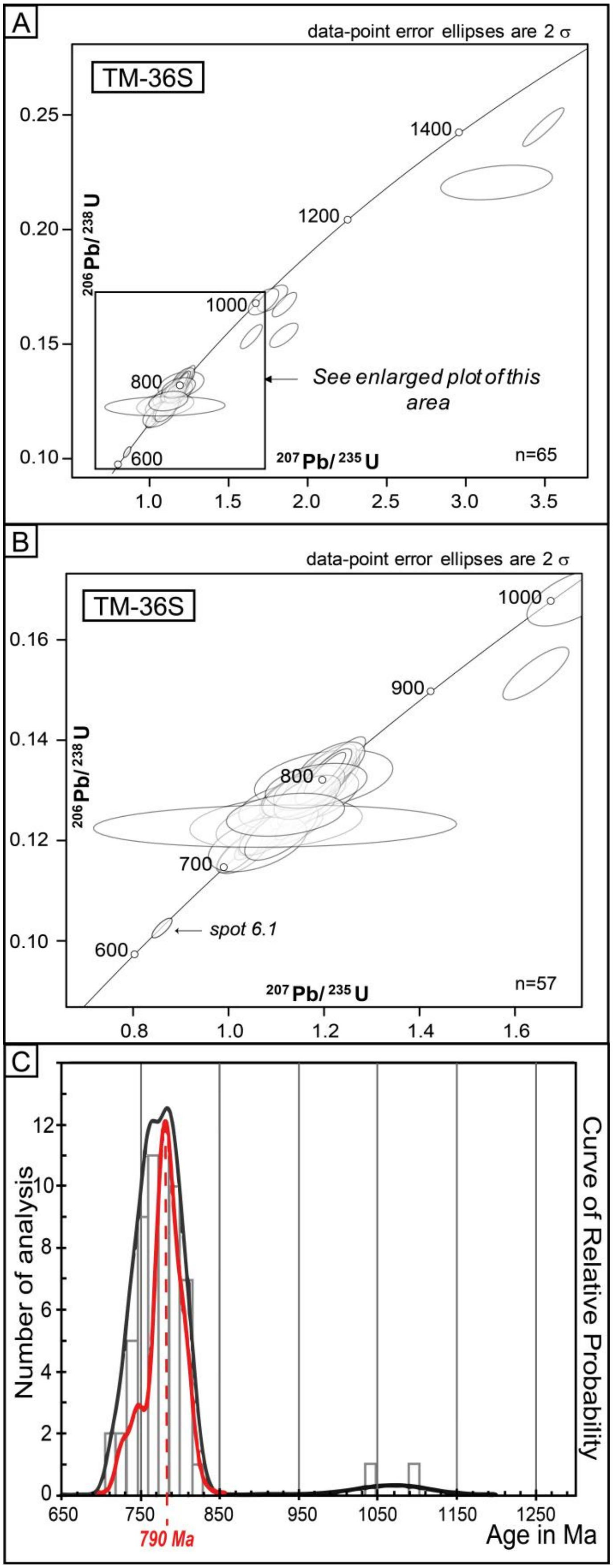

Figure 7. A) Concordia U-Pb diagram with all zircons analysed from paragneiss sample TM-36S; B) Zoom in Fig. 7A, showing the Neoproterozoic population of detrital zircons; C) Histogram with the

detrital zircon population of sample TM-36S (in black). Note the curve of relative probability for TM-36S compared to the relative probability curve of the igneous zircons from the orthogneiss sample TM-36F (in red). The calculated crystallisation age of the orthogneiss is shown as a dashed red line.

5.3. Metarhyolite (TM-26A)

Sample TM-26A shows zircons 100 to 300 µm long with elongate prismatic habits and well-preserved to sub-rounded bipyramidal tips (Fig. 8a). Some zircon grains display darker cores, sometimes with well-defined oscillatory zoning. The U-Pb ages reveal that the rounded cores are inherited zircon grains, and the oscillatory-zoned overgrowths or rims represent magmatic zircon.

Twenty-three SHRIMP analyses were performed on fifteen different zircon grains, and the resulting data were plotted in a conventional Wetherill U–Pb concordia diagram (Fig. 8b, c). In this dataset, 17 spots represent the most concordant analyses, whereas the data with discordance higher than 5% were excluded. Fifteen analyses of grains, with Th/U ratios between 0.26 and 0.67, define a concordia age of 787 ± 5 Ma (2σ), which is interpreted as the best estimate for crystallisation of the volcanic protolith (Fig. 8c).

Although most of the analyses on xenocrystic cores yielded highly discordant data, two spots (#11.2 and #14.2 - Th/U ratios of 0.65 and 0.44 – Fig. 8a) yielded nearly concordant data suggesting ages of *ca.* 2.0 Ga. Both also have oscillatory overgrowths of ca. 760 Ma, suggesting that the protolith age of crystallisation is Tonian, and the Paleoproterozoic core might indicate a source partially melted during the Tonian magmatic event.

The other two spots with discordance <10% yielded $^{206}Pb/^{238}U$ dates represent inheritance (Fig. 8b). Spot #2.1 gave a date around 2.0 Ga; however, the Th/U ratio is relatively low (0.03) compared to the inherited concordant cores of similar age. Spot #8.1 indicates a core of approximately 2.5 Ga and a Th/U ratio of 0.62.

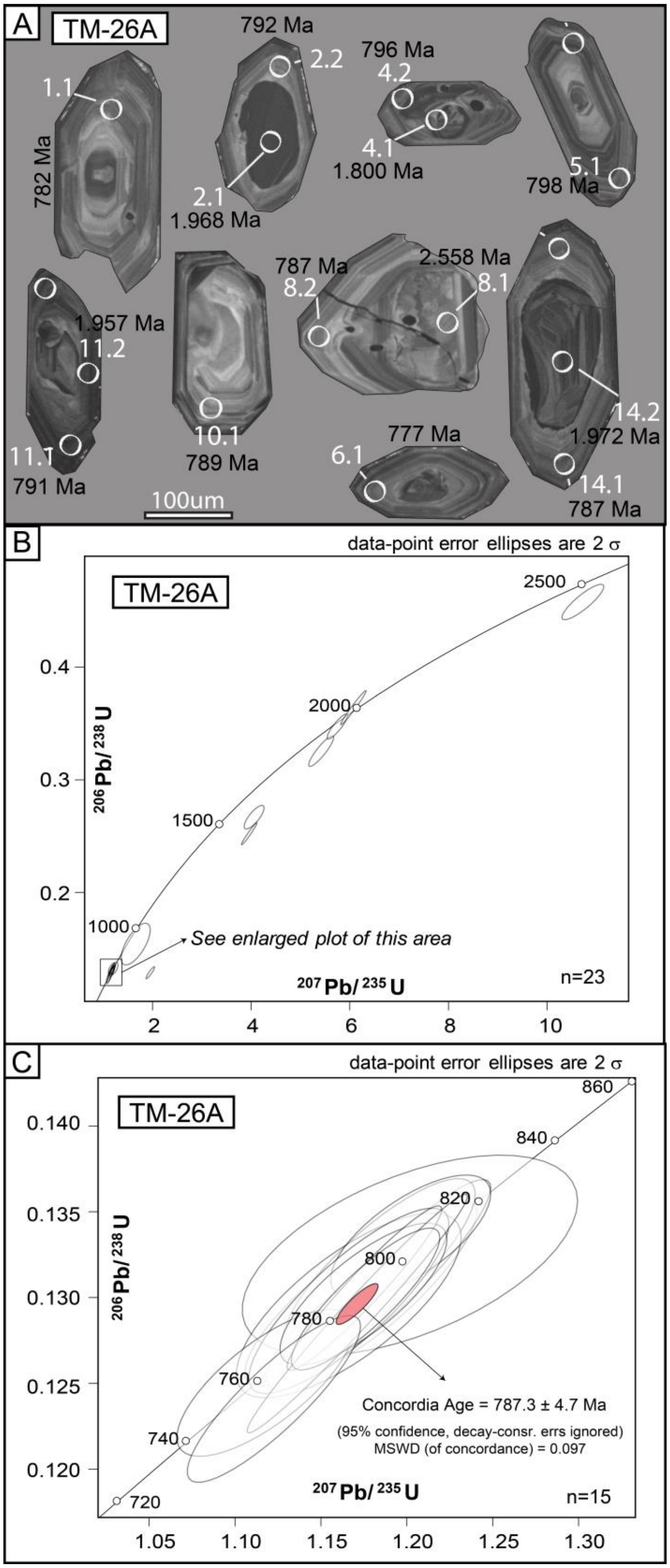

Figure 8. A) Cathodoluminescence images from some zircon crystals of Porongos Complex blastoporphyritic metarhyolite sample TM-26A, (ages are given as $^{206}Pb/^{238}U$ – complete information is available as supplementary data). Note the inherited core on crystals #2.1, #4.1 and #14.2. B)

Concordia U-Pb diagram with all zircons analysed from sample TM-26A. C) Neoproterozoic zircons enlarged plot, where the concordia age is interpreted to be this rocks's crystallisation age.

6. OXYGEN ISOTOPES RESULTS

Oxygen isotope studies in zircon crystals are important allies to elucidate processes during magma evolution (Eiler, 2001; Valley et al., 2005; Scherer et al., 2007). A single zircon grain may even register more than one process, which is commonly marked by its zones or intergrows (Scherer et al., 2007). Therefore, whenever possible, the U–Pb ratios and the $\delta^{18}O$ values were determined in the same spot to correlate the $\delta^{18}O$ values with the U–Pb age of the analysed grain. The four studied samples show similar $\delta^{18}O$ values, most commonly ranging from 7.9‰ to 9.7‰ (Fig. 9a). $\delta^{18}O$ values lower than 7 were registered in all samples, but values lower than "mantle values" ($\delta^{18}O$ mantle = 5.3±0.3‰ – Valley et al., 1998) were only measured in sample TM-36S (VCC para-derived gneiss). Only one analytical spot in the PC sample (TM-26A) yielded a $\delta^{18}O$ value typical for the mantle zircon crystal. The highest $\delta^{18}O$ value found in the VCC samples is 9.4‰, registered in the ortho-derived gneiss TM-36F (Fig. 9b), whilst the highest value in the PC sample TM-26A is 10.2‰ (Fig. 9c).

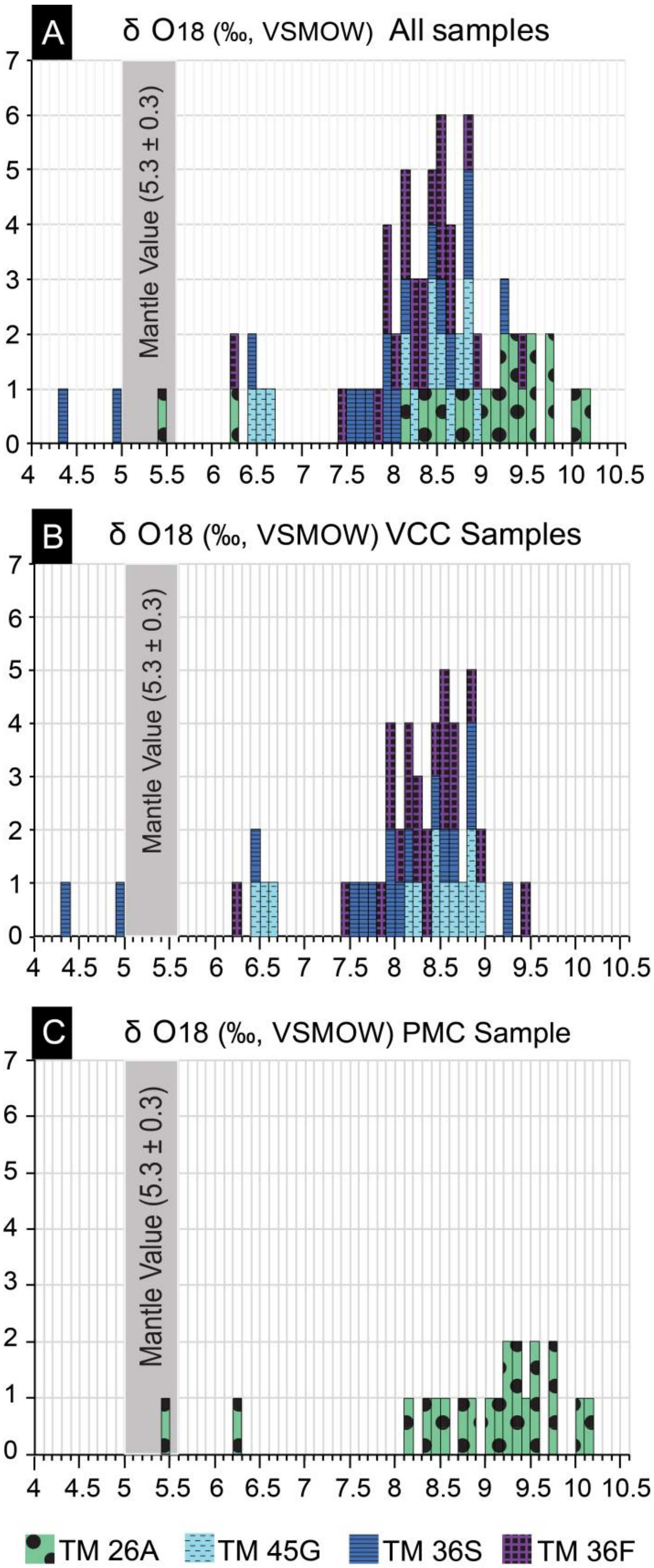

Figure 9. Zircon oxygen isotopic values measured in the four studied samples. A) $\delta^{18}O$ zircon values from all samples; B) $\delta^{18}O$ zircon values from Várzea do Capivarita Complex samples; C) $\delta^{18}O$ zircon values from Porongos Complex sample.

Most of the spots were performed on Neoproterozoic igneous zircons, either on their cores or rims (Fig. 10). Crystal cores (Fig. 10a) and crystal rims (Fig. 10b) generally show similar $\delta^{18}O$ values, although they present some differences. For example, in the PC sample TM-26A, $\delta^{18}O$ values measured in some zircon rims are slightly higher than values from zircon cores of the same sample. Conversely, in the para-derived VCC gneiss TM-36S, the calculated mean $\delta^{18}O$ values are much smaller in crystal rims (6.45±1.48‰) than in crystal cores (8.03±0.33‰). Nevertheless, the large statistical error and standard deviation indicate that these data require caution since only two spots were analysed in zircon rims of sample TM-36S (Fig. 10b). Mean $\delta^{18}O$ values with their error, standard deviation and number of analysed spots (n) for each sample are shown in figure 10, where 10a only presents the data from igneous zircons cores; 10b presents the data from igneous zircons rims and in 10c is showed all statistical data together (zircons core + zircons rims). Examples of analysed zircon in each sample are also shown as cathodoluminescence images, where each spot's U-Pb age and $\delta^{18}O$ value are indicated (Fig. 10). All analysed spots are available as supplementary data.

As described above, inherited zircons cores were registered in all studied samples. In order to compare them with Neoproterozoic igneous zircons, $\delta^{18}O$ values were also measured in some of these inherited zircon cores. The results are indicated in figure 10d, with their statistical data and some examples of analysed spots. As expected, many of the smallest $\delta^{18}O$ values found in the studied samples are related to inherited zircons (Fig. 10d). However, two points do not follow the expectations: 1) the smallest $\delta^{18}O$ value in sample TM-36S is related to Neoproterozoic igneous zircon and not to inherited population; 2) despite the smallest $\delta^{18}O$ value of the sample TM-26A be from an inherited zircon, one spot performed in inherited zircons gave $\delta^{18}O$ value (10.2‰) higher than those found to the igneous zircons ($\delta^{18}O$<10.1‰).

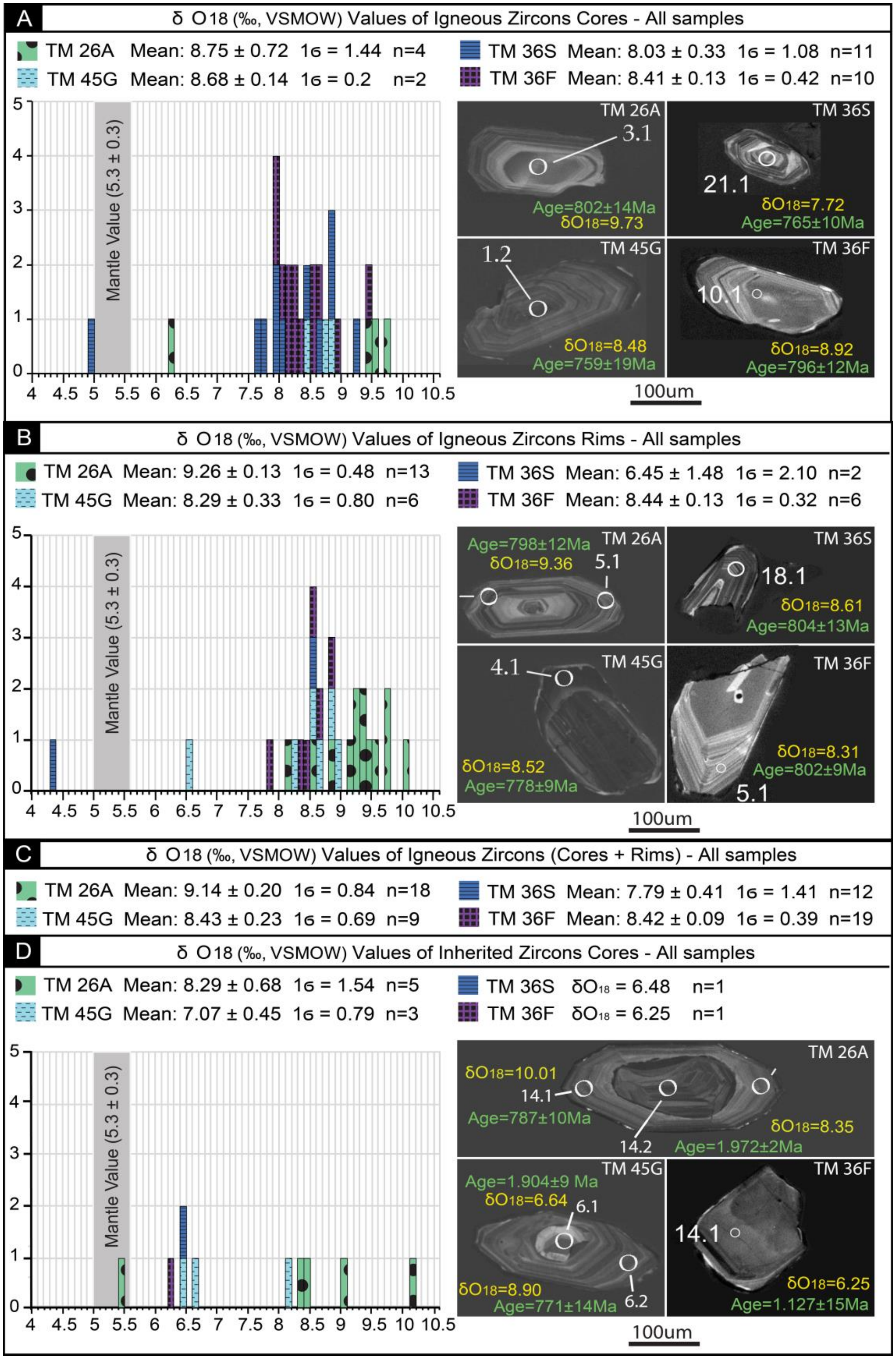

Figure 10 - δ^{18}O values: A) Data from spots analysed in Neoproterozoic zircon cores, B) Data from spots analysed in Neoproterozoic zircon rims. C) General δ^{18}O zircon values, considering all measured data (core spots + rim spots). D) δ^{18}O values measured in inherited zircons cores.

The correlation of $\delta^{18}O$ values with the U-Pb ages of analysed zircon crystals, considering only the U-Pb ages with less than 5% of discordance, show no statistical correlation (Fig. 11a). Inherited zircons (older than 1000 Ma, in figure 11a) have $\delta^{18}O$ values from 6.3‰ to 10.2‰. The studied Neoproterozoic igneous zircons of 800-750 Ma have commonly $\delta^{18}O$ values higher than 7.5‰ to slightly higher than 10‰. Few values around 6.5‰ and smaller than 5‰ are also reported. In figure 11a, the magmatic zircon evolution curve is shown through the geological time (Valley et al., 2005), in which the highest expected magmatic $\delta^{18}O$ values to a given age are delimited by the curve, according to Valley et al. (2005). In other words, magmatic zircons should plot under the curve. However, as shown in figure 11a, two inherited zircons from PC sample TM-26A (#2.1 and #11.2) have plotted above such a curve and will be discussed later.

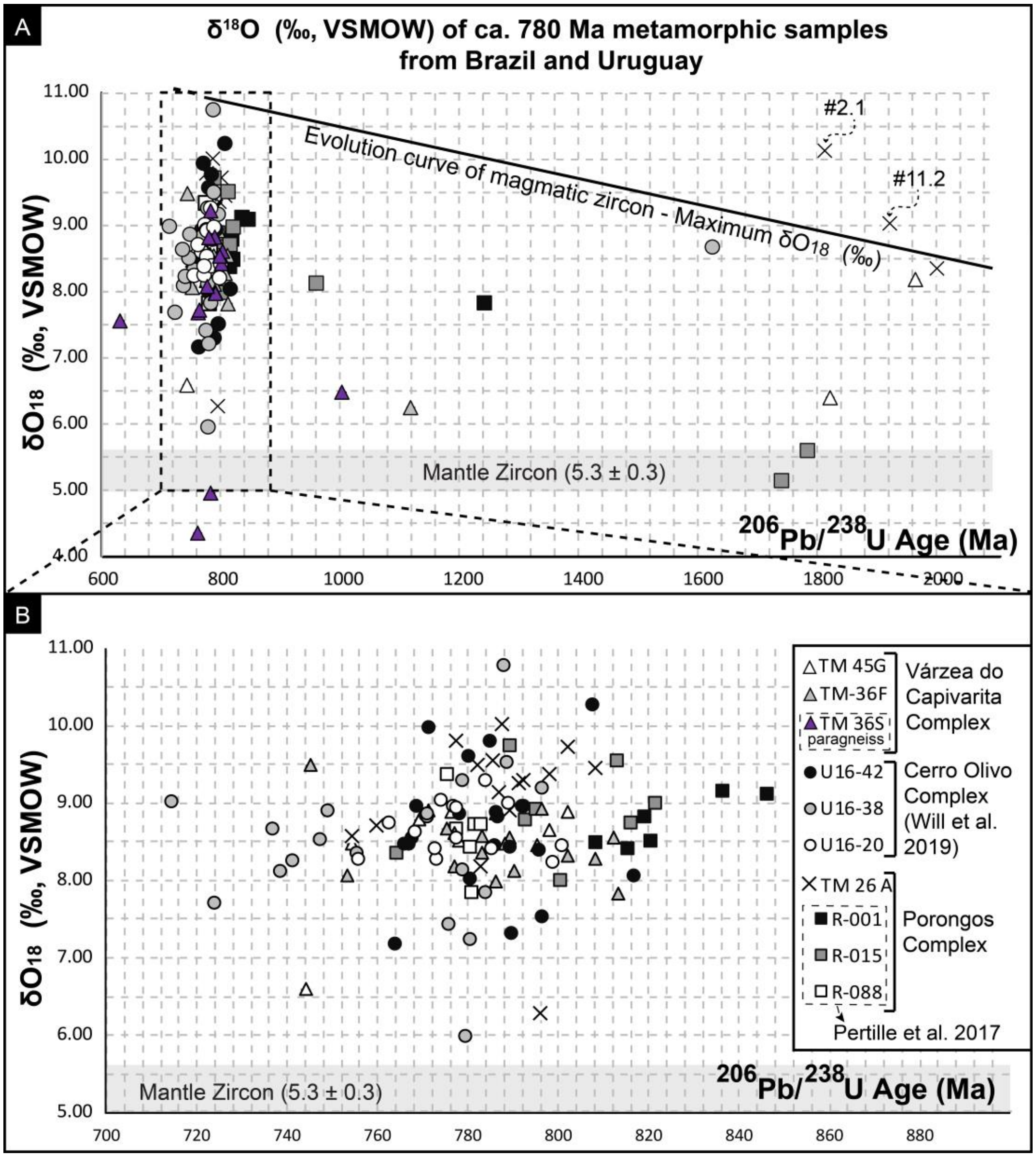

Figure 11 – A) δ^{18}O zircon values plotted against the magmatic age of the grains (spots #2.1 and #11.2 are indicated – see text for further information). The magmatic zircon evolution curve through geological time (Valley et al., 2005) suggest the highest expected magmatic δ^{18}O values to a given age. B) Comparison of δ^{18}O zircon values between ca. 770-800 Ma ortho-derived metamorphic rocks from Brazil (Várzea do Capivarita Complex, Porongos Complex) and Uruguay (Cerro Olivo Complex).

7. DISCUSSION

7.1. *Timing of pre-collisional igneous events in the hinterland and foreland of the Dom Feliciano Belt*

The new geochronological data obtained for the Várzea do Capivarita Complex orthogneisses demonstrate the Tonian age of their protolith, with Meso- to Paleoproterozoic inheritance ages, and reveal that such rocks are related to a magmatic event at ca. 790 Ma, in the DFB hinterland. The tonalitic orthogneiss (TM-36F) yielded a concordant U-Pb SHRIMP age of 786 ± 5 Ma (2σ) with one ca. 1.1 Ga inherited zircon. Likewise, the granitic orthogneiss (TM-45G) yielded the same (within error) mean $^{206}Pb/^{238}U$ SHRIMP age of 780 ± 10 Ma with ca. 1.8 and 2.0 Ga inherited zircon xenocrysts. This magmatic event has the same age interval reported for the protoliths of granulitic orthogneisses in the Cerro Olivo Complex (COC) within the Uruguayan part of the DFB, further south along strike (Fig.1). The U–Pb SHRIMP ages for COC are ca. 780 Ma (Will et al., 2019), 802–767 Ma (Lenz et al., 2011), 782 ± 7 Ma (Masquelin et al., 2011), 761 ± 7 (Basei et al., 2011), 776 ± 12 Ma (Oyhantçabal et al., 2009), and 762 ± 8 (Hartmann et al., 2002). In the Brazilian part of the DFB, high-grade igneous rocks with ca. 800-770 Ma protolith ages were discussed in the central sector of the belt by Koester et al. (2016) and Martil et al. (2017), and in its northern sector by De Toni et al. (2020b).

The Porongos Complex metarhyolite yielded a concordant U–Pb SHRIMP crystallisation age of 787 ± 5 Ma (2σ) with inheritance at ca. 2.0 Ga. Such age and the Th/U ratios obtained in these igneous zircon grains are similar to those of the VCC (Table 1). Our data represent the first published dating of the metavolcanics lying at the PC easternmost border (Fig. 2). The geochemical similarities of all samples studied in this paper were pointed out by Martil et al. (2017) and Battisti et al. (2018). The obtained age for the PC metarhyolite falls within the time interval of 800-770 Ma for pre-collisional magmatic events in the PC established by previous studies (Soliani

Jr, 1986; Saalmann et al., 2011; Pertille et al., 2017). Thus, our result is coherent and confirms that the ca. 790 Ma magmatism was also important in the DFB foreland. In our view, this magmatism is mainly found eastwards of the Santana da Boa Vista thrust fault (see further discussion). Furthermore, our geochronological data in meta-igneous rocks demonstrate that magmatic activity has taken place in the hinterland and foreland of the DFB at ca. 790 Ma. Such data imply that the contact between the Eastern Domain - where Várzea do Capivarita is usually placed (Fig. 1 and 2), and the Central Domain - where Porongos Complex is located, does not represent a tectonic border of distinct terranes (*stricto sensu, i.e. allochthonous*) in the DFB Central Sector, as commonly referred in the literature.

INSERT TABLE 1

7.2. Syn-volcanic sedimentation in the Várzea do Capivarita Complex

Provenance studies in the paragneiss sample (TM-36S) demonstrate the main detrital population between ca. 790 and 750 Ma. Such detrital population is coeval with the magmatic event that generated the protoliths of the orthogneisses TM-36F and TM-45G from the same complex (Fig. 7c). The time interval of 790-750 Ma is also coeval with the igneous protolith ages reported in the literature for the Cerro Olivo Complex in Uruguay, as shown in item 7.1 (Hartmann et al., 2002; Oyhantçabal et al., 2009; Lenz et al., 2011; Basei et al., 2011; Masquelin et al., 2011; Will et al., 2019). The coincidence of ages in the VCC ortho- and paragneisses may be interpreted in two alternative ways. The protolith of the paragneiss sample originated as volcanoclastic debris, as in arc settings, for instance, or was deposited in a tectonically very active environment, with rapid exhumation, erosion and deposition in a rift setting. Both alternatives suggest short transport of detritus that would explain the preservation of the pyramidal tips of the detrital zircons (Fig. 5). However, the first hypothesis is preferred based on the geochemical signature of the VCC orthogneisses, which is compatible with that found in a mature magmatic arc setting (Martil et al., 2017).

The similar morphology and age of the igneous and detrital zircon crystals from the studied VCC samples strongly suggest that at least part of this unit may represent metamorphosed syn-sedimentary volcanic or volcano-sedimentary deposits. This dataset also implies that the interleaving of orthogneiss and paragneiss in the VCC represents, at least in part, its original S_0, which might have also been interleaved tectonically later, during the transpressive deformation. The high metamorphic grade (granulite facies) and intense deformation that affected these rocks have obliterated any additional depositional features of the protoliths that would permit a better interpretation of their mutual relationships. One single spot (#6.1) in a zircon grain from the paragneiss sample TM-36S yielded an age of 632 ± 9 Ma, which is interpreted as related to such metamorphic granulite facies event, based on its distinct morphology and low Th/U ratio (0.01). The same metamorphic event is registered in the orthogneiss TM-36F, where a single spot (#15.1), 8% discordant, has $^{206}Pb/^{238}U$ age of 625±6 Ma. This interpretation is in agreement with the well-known time interval for the main collision in the DFB at ca. 650–620 Ma (Gross et al., 2006, 2009; Oyhantçabal et al., 2009; Chemale et al., 2011; Lenz et al., 2011; Basei et al., 2011; Philipp et al., 2016a; Peel et al., 2018; Will et al., 2019; Percival et al., 2022).

According to Gruber et al. (2016a), the maximum depositional age for the VCC clastic sedimentary rocks is 728 ± 11 Ma (U–Pb SHRIMP), and an interval of ca. 717–750 Ma ($^{87}Sr/^{86}Sr$ whole rock) is proposed for the marble sequence deposition. Considering the error and the small number of grains, our data (two detrital grains with 716±10 and 717±9 Ma, respectively) corroborate the maximum VCC depositional age interpretation.

7.3. *Interpretation and correlation of the zircon oxygen isotopic data*

The reliability of geochronological data from high-grade rocks, such as in the VCC and COC, is discussed in the literature, as in the Harts Range Group, Australia, for example (Maidment et al., 2013). Such preservation is common in zircon due to the extremely low diffusion rates of Pb, Th and U in the crystal lattice, even at high temperature and pressure (Lee et al., 1997; Cherniak and Watson, 2001, 2003; Scherer et al., 2007). The diffusion rate of oxygen in zircon under high-temperature conditions is also low (Peck et al., 2003), with effective closure temperatures at around 700°C (Watson and Cherniak, 1997), and suggests that $\delta^{18}O$ values are reliable even in high-grade metamorphic rocks (e.g. Valley et al., 1994). However, in extreme cases, radiation damage, metamictisation and micro fracturing could facilitate the late exchange of oxygen (Valley, 2003).

As established by Valley et al. (1998) and discussed by Bindeman (2008), among many other authors, zircon in equilibrium with mantle-derived melts has an average $\delta^{18}O$ value of 5.3 ± 0.3‰. Higher $\delta^{18}O$ values reflect the presence of ^{18}O-enriched components such as the melting or assimilation of crustal material or hydrothermally altered oceanic crust (Peck et al., 2001; Valley et al., 2005; Kemp et al., 2006). Such $\delta^{18}O$ enrichment process results in an expected “evolutionary curve of magmatic zircons” over the geological time (Fig. 11) (Valley et al., 2005). As predicted by this curve, $\delta^{18}O$ values higher than 7.5‰ are not recorded in igneous zircons older than 2.5 Ga, but they are common in zircon crystallised in the Proterozoic times. Lastly, zircon crystals could also present $\delta^{18}O$ values lower than 5‰. Such values commonly represent shallow sub-volcanic magma chambers where low $\delta^{18}O$ values resulted from the melting of hydrothermally altered wall rock (Bindeman and Valley, 2000; Valley, 2003; Valley et al., 2005) or, less often, from the contribution of glacial ice melting in rifting scenarios (Wickham and Taylor, 1985), since meteoric water has negative (to strongly negative) $\delta^{18}O$ values.

Our data demonstrate that $\delta^{18}O$ values from VCC and PC samples are quite similar, where the most common $\delta^{18}O$ values range between 7.9‰ and 9.7‰. $\delta^{18}O$ lower than 7.5‰ were registered in all studied samples, in which four of these spots are related to the Neoproterozoic zircon population. Two of these spots are from the paragneiss TM-36S (#24.1 and #20.1 - all analysed spots are available as supplementary data). Because they are preserved in a paragneiss, they could represent a minor detrital contribution from neighbouring sources, and thus, these two grains may not provide reliable information for further interpretations of the VCC syn-volcano-sedimentary scenario. Nevertheless, the two other spots with $\delta^{18}O$ values of 6.5‰ and 6.2‰ were registered in the orthogneisses TM-45G and TM-26A, respectively (Fig. 9). Such values could be easily explained by a lower-$\delta^{18}O$ mantle-derived input (Valley, 2003). Moreover, some hydrothermal water could also be responsible for reducing the $\delta^{18}O$ values of such Neoproterozoic grains (Bindeman and Valley, 2000). However, the crystals do not show any cracks to permit such interaction. Irrespective of the meaning of those lower $\delta^{18}O$ zircons, only a few grains record such effect, which suggests that it was not a significant event.

The highest value of $\delta^{18}O$ found in the VCC samples is 9.4‰ in a zircon core of TM-36F (VCC orthogneiss). On the other hand, the highest $\delta^{18}O$ values of the PC sample are mostly related to the igneous zircon rims. Surprisingly, the highest value for the PC sample was found in the core of an inherited zircon (1.96 Ga): $\delta^{18}O = 10.2‰$ (Fig. 9) (spot #2.1-supplementary data). Spot #2.1 is 9% discordant, it has a relatively low Th/U ratio (0.03), and in figure 11, plots above the “evolutionary curve of magmatic zircons”. Such indications mean that this zircon is non-magmatic or, most probably, a magmatic zircon affected by a younger hydrothermal or metamorphic event. As the low Th/U ratio suggests, the latter alternative is more probable. Spot #11.2 also plots above the expected curve (Fig. 11). However, it is 2% discordant and has a Th/U ratio equal to 0.65, which suggests an igneous origin for this grain.

As shown in figures 10 and 11, only one inherited zircon crystal has crystallised in equilibrium with mantle $\delta^{18}O$ values. The vast majority of the analysed zircon grains have higher $\delta^{18}O$ values following the expected evolution curve for magmatic zircon of Valley et al. (2005). The main calculated $\delta^{18}O$ for Neoproterozoic igneous zircons in all studied samples, summarised in table 1, also show higher than mantle $\delta^{18}O$ values. Such data suggest that most zircons crystallised in more evolved magmas, either as a response to the melting of host rocks and sediments (buried and/or subducted) or as a response to the assimilation of crustal material by mantle-derived magmas, as by assimilation-fractional crystallisation (AFC) processes (Peck et al., 2001; Valley, 2003; Kemp et al., 2006). Further discussions regarding the magmatic processes using $\delta^{18}O$ data would require additional sampling of a larger SiO_2 range (magmatic series) to correlate the fractionation of zircon $\delta^{18}O$ in comparison to whole-rock $\delta^{18}O$ values.

The crystallisation of zircon from more evolved magmas is also registered in the available $\delta^{18}O$ data from the literature, acquired in other ortho-derived rocks from DFB central and southern sectors with ca. 800-770 Ma protolith age. This is demonstrated in Figure 11, where our present VCC and PC data are compared with three other PC acid metavolcanic samples (Pertille et al., 2017) and three granulitic orthogneiss samples from the Cerro Olivo Complex in Uruguay (Will et al., 2019).

7.4. *Shared pre-collisional evolution of Dom Feliciano Belt hinterland and foreland units*

The coeval protolith ages obtained for the Várzea do Capivarita Complex (TM-36F, TM-45G) and the Porongos Complex (TM-26A) samples pointed out age similarities of part of the protoliths in both units (table 2 and 3). Such temporal connection, together with the geochemical and structural results of Martil et al. (2017) and Battisti et al. (2018), has strengthened our interpretation that both complexes represent different parts of a single basin at some point in their geological history. According to our geochronological data from meta-igneous rocks, this connection was likely at 790–780 Ma.

Nevertheless, it should be noted that the PC western region contains younger metavolcanic rocks (e. g. Höfig et al., 2018) and also younger sources of detrital material than its eastern region, as shown by Pertille et al. (2015a, 2017), Gruber et al. (2016b) and Höfig et al. (2018). Furthermore, these data reflect distinct evolutionary histories for the western and eastern regions of the PC, as discussed by Battisti (2022). For these reasons, the data discussed here indicate a direct correlation only between the VCC and the PC eastern region, but not the PC as a whole. The geochronological differences between the western and eastern PC rocks are summarised in tables 2 and 3 and figure 2. Aiming to compare DFB units, tables 2 and 3 also show the data from granulitic rocks of the Cerro Olivo Complex in Uruguay.

As seen in Figure 11, the $\delta^{18}O$ values in zircon also demonstrate a direct correlation between ortho-derived samples from the VCC and PC eastern region. Moreover, zircon $\delta^{18}O$ also points out a correlation between the ca. 800-770 Ma magmatic event in Brazil and Uruguay, as already suggested in other geochronological, isotopic and structural studies (e.g. Basei et al., 2000; Martil et al., 2017; Konopásek et al., 2018; De Toni et al., 2020b).

INSERT TABLE 2

INSERT TABLE 3

While the correlations among various meta-igneous rocks of early Neoproterozoic age are straightforward, the correlation of metasedimentary rocks from the PC and VCC requires more caution. That is because the detrital provenance in the PC rocks is much better studied than in the VCC ones. However, keeping this in mind, some considerations can be made. Both complexes present a similar detrital interval for pre-collisional metasedimentary rocks: 750 Ma – 3.0 Ga for PC (Gruber et al., 2016b; Pertille et al., 2017; Höfig et al., 2018), and 730 Ma – 2.5 Ga for VCC (Gruber et al., 2016a). Regarding the main age peaks, the PC rocks show two main peaks (1.2–1.5 and 2.0–2.3 Ga), while the VCC samples show only one well-marked peak at 1.9–2.2 Ga (Gruber et al., 2016a). Moreover, the pronounced ca. 790 Ma age peak found in the paragneiss TM-36S has not yet been registered in the VCC metasedimentary rocks, although individual data showing such detrital age were reported by Gruber et al. (2016a) also in other parts of the VCC. The latter two differences may be explained by a shortage of data from the VCC, and we interpret that the absence of age peaks at ca. 1.2-1.5 Ga in the VCC will probably be solved when more studies are available. Therefore, despite the caution in interpreting the relationship between the para-metamorphic rocks, they also suggest a shared depositional origin by VCC and PC, indicated by our data in the ortho-metamorphic rocks of both complexes.

The geological setting of the ca. 800-770 Ma DFB metaigneous rocks is debatable. Two main interpretations are found in the literature, and for this reason, a continental arc (Koester et al., 2016; Martil et al., 2017; De Toni et al., 2020b) or a back-arc/rift setting (Konopásek et al., 2018, 2020; Will et al., 2019) are assumed as possible environments. Models aiming to reconcile both interpretations are found in the recent literature (e.g. De Toni et al., 2020b; Hueck et al., 2022). Geochemical and isotopic features favour the first hypothesis (Martil et al., 2017; De Toni et al., 2020b), and the structural data are not discriminant. Although this discussion is not the focus of the present work, our zircon data demonstrate that the generation of 800-770 protoliths has involved contamination/assimilation of crustal material, which is very likely in both scenarios. Therefore, it is important to highlight that our proposed VCC-PC syn-volcano-sedimentary environment is not exclusive of either a continental arc or a back-arc/rift, and it is supported in both scenarios, as shown in figure 12.

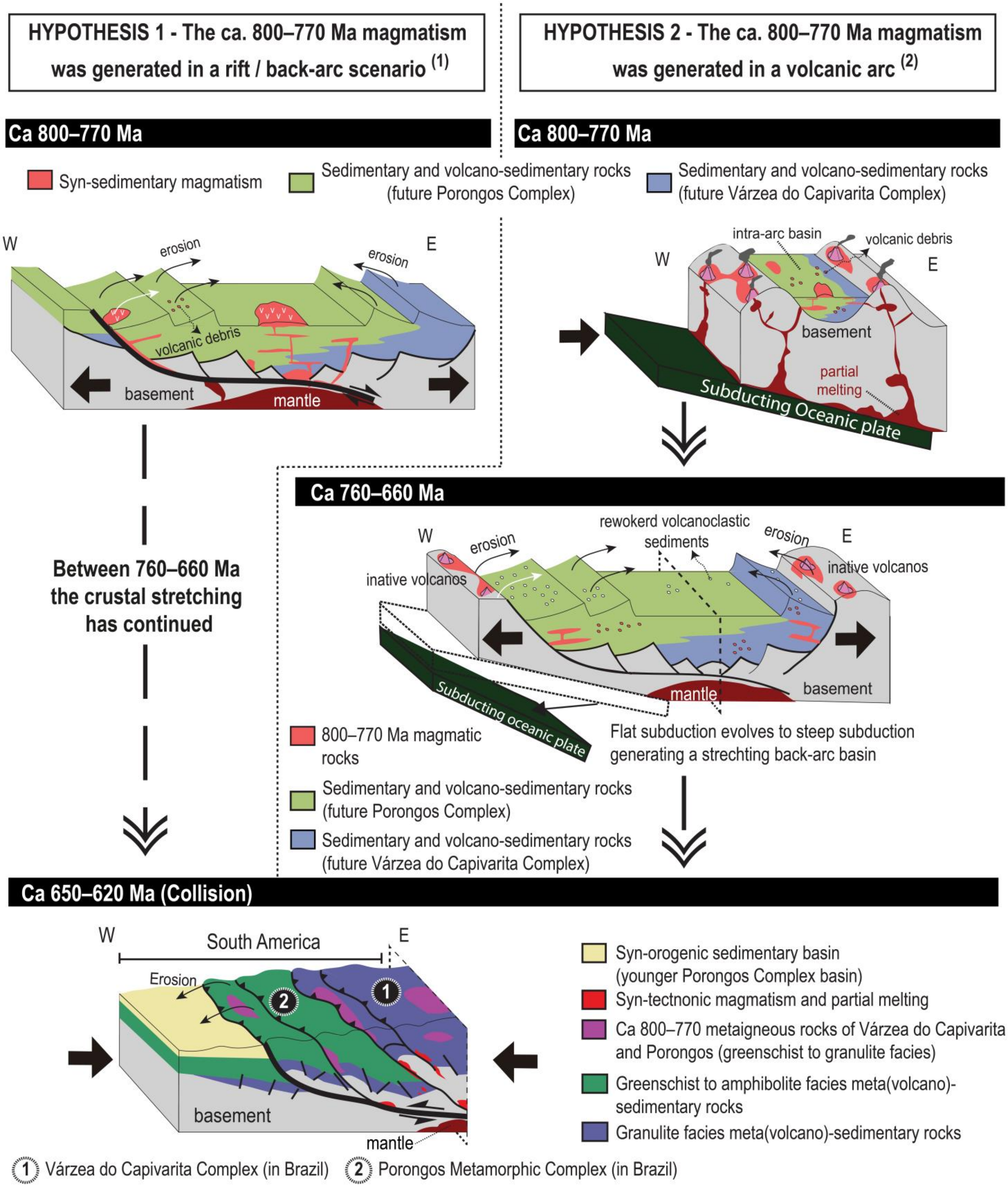

Figure 12. Models proposed in the literature for the study region: Hypothesis 1 is an idealised drawing after the discussion of Konopásek et al. (2020), in which a rift/back-arc scenario was responsible for

generating 800-770 Ma VCC, PC and COC ortho-protoliths. Hypothesis 2 is redrawn from De Toni et al. (2020b), in which the authors propose arc magmatism as the best scenario for the emplacement of 800-770 Ma VCC, PC and COC ortho-protoliths. The syn-volcano-sedimentary environment proposed in this paper is achievable in both situations, irrespective of the chosen model.

Thus, our geochronological and isotopic data suggest that at least part of the VCC represents former sedimentary rocks that originated through erosion of coeval igneous rocks. Furthermore, the similar age and isotopic record of zircon in the VCC and PC meta-igneous samples raises the hypothesis that the Várzea do Capivarita Complex and part of the Porongos Complex represent different portions of a former single volcano-sedimentary basin (Fig. 12). This basin was inverted at ca. 650 Ma by progressive dextral/top-to-W transpressive deformation resulting in exhumation and thrusting of its deeper and hotter part (VCC) over its margins (PC) (Fig. 12). However, the contact between VCC and PC is now obliterated by younger magmatic activity. After the basin inversion, such contact was probably represented by thrust faults, as discussed in Battisti et al. (2018). The age of ca. 650–620 Ma for this inversion event is supported by several authors in Brazil (in VCC: Gross et al., 2006; Chemale et al., 2011; Martil, 2016; Philipp et al., 2016; in PC: Lenz, 2006, Battisti, 2022 and in Uruguay Gross et al., 2009; Oyhantçabal et al., 2009; Lenz et al., 2011; Basei et al., 2011; Peel et al., 2018; Will et al., 2019). The relationship between the high-grade Uruguayan rocks and VCC–PC basin is more obscure. However, our isotopic comparison and many other isotopic and geochronological data from the literature show that the generation of all these rocks is probably the result of the same tectono-magmatic evolution.

8. CONCLUSIONS

The results obtained from geochronological U–Pb SHRIMP and oxygen isotope data in zircon from two orthogneiss samples and one paragneiss of the Várzea do Capivarita Complex, in addition to one metarhyolite sample of the Porongos Complex from the central sector of the Dom Feliciano Belt, southernmost Brazil, allow us to draw the following conclusions:

i) The Várzea do Capivarita Complex (VCC) has, at least in part, a syn-volcano–sedimentary origin at ca. 790 Ma.

ii) The geochronological dataset of the paragneiss sample constrains a maximum depositional age of 716 ± 10 Ma for the VCC original basin.

iii) The geochronological and zircon oxygen isotopic similarities shown for the VCC and Porongos Complex (PC) samples imply igneous protoliths for these complexes.

iv) Várzea do Capivarita Complex and part of the Porongos Complex (mostly its eastern region) have represented different parts of a single basin at ca. 800-770 Ma. Therefore, such dataset plays against the possibility of these complexes representing distinct tectonic terranes (*stricto sensu, i.e. allochthonous*) of the Dom Feliciano Belt, as commonly referred in the literature.

v) The $\delta^{18}O$ zircon data demonstrate that most ca. 800-770 Ma protoliths of the VCC and PC metaigneous rocks have crystallised in more evolved magmas, either from the melting of host rocks and sediments or assimilation of crustal material by mantle-derived magmas.

vi) A connection between the ca. 800-770 Ma protoliths of the Cerro Olivo Complex, in the southern sector of the Dom Feliciano Belt, and the VCC–PC basin in the central sector is supported by geochronological and zircon isotopic oxygen data presented in this study.

ACKNOWLEDGEMENTS

The authors acknowledge Coordenação de Aperfeiçoamento de Pessoal Docente for funding of the CAPES (Brazil) – SIU (Norway) cooperation program (CAPES -

88881.117872/2016-01 and 88887.141226/2017–00, SIU – TF-2016-CAPES-SIU/10024). MAB thanks the Brazilian National Research Council (CNPq) for the PhD scholarship; MFB acknowledges CNPq for Productivity Grant 311501/2019-2; RSS thanks CNPq for research grant 311748/2018-0; JK appreciates financial support of the Czech Science Foundation (grant no. 18-24281S). The authors are grateful to Sebastián Oriolo, an anonymous reviewer, and the Precambrian editors, whose critical reviews and comments have led to significant improvement of the manuscript.

REFERENCES

Arena, K.R., Hartmann, L.A., Lana, C., 2016. Evolution of Neoproterozoic ophiolites from the southern Brasiliano Orogen revealed by zircon U-Pb-Hf isotopes and geochemistry. Precambrian Res 285, 299–314. https://doi.org/10.1016/j.precamres.2016.09.014

Arena, K.R., Hartmann, L.A., Lana, C., 2018. U–Pb–Hf isotopes and trace elements of metasomatic zircon delimit the evolution of neoproterozoic Capané ophiolite in the southern Brasiliano Orogen. Int Geol Rev 60, 911–928. https://doi.org/10.1080/00206814.2017.1355269

Arena, K.R., Hartmann, L.A., Lana, C., 2017. Tonian emplacement of ophiolites in the southern Brasiliano Orogen delimited by U-Pb-Hf isotopes of zircon from metasomatites. Gondwana Res 49, 296–332. https://doi.org/10.1016/j.gr.2017.05.018

Basei, M., Siga, O., Masquelin, H., Harara, O., Reis Neto, J., Preciozzi, F., 2000. The Dom Feliciano belt (Brazil-Uruguay) and its foreland (Rio de la Plata Craton): framework, tectonic evolution and correlations with similar terranes of southwestern Africa, in: Cordani, U.G. (Ed.), Tectonic Evolution of South America. 31st International Geological Congress, Rio de Janeiro, Brazil, pp. 311–334.

Basei, M.A.S., Frimmel, H.E., Campos Neto, M. da C., de Araujo, C.E.G., de Castro, N.A., Passarelli, C.R., 2018. The Tectonic History of the Southern Adamastor Ocean Based on a Correlation of the Kaoko and Dom Feliciano Belts. pp. 63–85. https://doi.org/10.1007/978-3-319-68920-3_3

Basei, M.A.S., Peel, E., Sánchez Bettucci, L., Preciozzi, F., Nutman, A.P., 2011. The basement of the Punta del Este Terrane (Uruguay): an African Mesoproterozoic fragment at the eastern border of the South American

Río de La Plata craton. Int J Earth Sci 100, 289–304. https://doi.org/10.1007/s00531-010-0623-1

Battisti, M.A., 2022. Evolução geológica (800-560 Ma) do setor central Do Cinturão Dom Feliciano com base no estudo petrológico, geocronológico e de proveniência dos complexos Porongos, Várzea Do Capivarita e Passo Feio, RS, Ph Thesis. Universidade Federal do Rio Grande do Sul, Porto Alegre - RS. In: http://hdl.handle.net/10183/239719

Battisti, M.A., Bitencourt, M. de F., De Toni, G.B., Nardi, L.V.S., Konopásek, J., 2018. Metavolcanic rocks and orthogneisses from Porongos and Várzea do Capivarita complexes: A case for identification of tectonic interleaving at different crustal levels from structural and geochemical data in southernmost Brazil. J South Am Earth Sci 88, 253–274. https://doi.org/10.1016/j.jsames.2018.08.009

Battisti, M.A., Bitencourt, M. de F., Schmitt, R. da S., Nardi, L.V.S., Martil, M.M.D., De Toni, G.B., Pimentel, M.M., Armstrong, R., Konopásek, J., 2022. Reconstruction of a volcano-sedimentary environment shared by the Porongos and Várzea do Capivarita complexes at 790 Ma, Dom Feliciano Belt, southern Brazil. Precambrian Res 378, 106774. https://doi.org/10.1016/j.precamres.2022.106774

Bicalho, V., Remus, M.V.D., Rizzardo, R., Dani, N., 2019. Geochemistry, metamorphic evolution and tectonic significance of metabasites from Caçapava do Sul, southern Brazil. Brazilian J Geol 49, 1–16. https://doi.org/10.1590/2317-4889201920180039

Bitencourt, M. de F., Nardi, L.V.S., 1993. Late- to Postcollisional Brasiliano Magmatism in Southernmost Brazil. An Acad Bras Cienc 65, 3–16.

Bitencourt, M. de F., Nardi, L.V.S., 2000. Tectonic setting and sources of magmatism related to the southern Brazilian shear belt. Rev Bras Geociencias 30, 184–187.

Bitencourt, M.F., 1983. Metamorfitos da região de Caçapava do Sul, RS – Geologia e Relações com o Corpo Granítico. Atas do 1º Simpósio Sul-Brasileiro Geol 37–48.

Bitencourt, M.F., Hartmann, L.A., 1984a. Geoquímica das Rochas anfibolíticas da região de Caçapava do Sul - RS - Parte 1: caracterização geológica e petrográfica, elementos maiores e menores. An DO XXXIII Congr Bras Geol 4266–4277.

Bitencourt, M.F., Hartmann, L.A., 1984b. Reconhecimento geoquimico dos xistos magnesianos da região do Passo Feio, Cacapava do Sul - RS. Congr Bras Geol (33   1984   Rio Janeiro, Rj) Anais Rio Janeiro   SBG, 1984.

Bitencourt, M.F., Nardi, L.V.S., Florisbal, L.M., Heaman, L.M., 2015. Geology, geochronology and petrogenesis of a Neoproterozoic, syntectonic sillimanite- muscovite-biotite granite from southernmost Brazil. B Abstr 8th Hutt Sympo- sium Granites Relat Rocks 179.

Boyton, W. V., 1984. Geochemistry of Rare Earth Elements: Meteorite studies, in: Henderson, P. (Ed.), Rare Earth Element Geochemistry. Elsevier, New York, p. 63.

Briqueu, L., Bougault, H., Joron, J.L., 1984. Quantification of Nb, Ta, Ti and V anomalies in magmas associated with subduction zones: Petrogenetic implications. Earth Planet Sci Lett 68, 297–308. https://doi.org/10.1016/0012-821X(84)90161-4

Chemale, F., Philipp, R.P., Dussin, I.A., Formoso, M.L.L., Kawashita, K., Berttotti, A.L., 2011. Lu–Hf and U–Pb age determination of Capivarita Anorthosite in the Dom Feliciano Belt, Brazil. Precambrian Res 186, 117–126. https://doi.org/10.1016/j.precamres.2011.01.005

Costa, A.F.U., 1997. Teste e modelagem geofísica da estruturação das associações litotectônicas pré-cambrianas no Escudo Sul-Rio-Grandense. PhD Thesis. Universidade Federal do Rio Grande do Sul, Porto Alegre, Brasil.

Costa, E.O. da, de Fátima Bitencourt, M., Tennholm, T., Konopásek, J., de Franceschi Moita, T., 2021. P-T-D evolution of the southeast Passo Feio Complex and the meaning of the Caçapava Lineament, Dom Feliciano Belt, southernmost Brazil. J South Am Earth Sci 103465. https://doi.org/10.1016/j.jsames.2021.103465

Costa, E.O. da, Gomes, E.M., Bitencourt, M. de F., De Toni, G.B., Nardi, L.V.S., 2020. Reassessing the PT conditions of Neoproterozoic collisional metamorphism and partial melting in southernmost Brazil. J South Am Earth Sci 100, 102584. https://doi.org/10.1016/j.jsames.2020.102584

De Toni, G.B., Bitencourt, M.D.F., Konopásek, J., Battisti, M.A., da Costa, E.O., Savian, J.F., 2021. Autochthonous origin of the Encruzilhada Block, Dom Feliciano Belt, southern Brazil, based on aerogeophysics, image analysis and PT-paths. J Geodyn 144. https://doi.org/10.1016/j.jog.2021.101825

De Toni, G.B., Bitencourt, M.F., Konopásek, J., Martini, A., Andrade, P.H.S., Florisbal, L.M., Campos, R.S., 2020a. Transpressive strain partitioning between the Major Gercino Shear Zone and the Tijucas Fold Belt, Dom Feliciano Belt, Santa Catarina, southern Brazil. J Struct Geol 104058. https://doi.org/10.1016/j.jsg.2020.104058

De Toni, G.B., Bitencourt, M.F., Nardi, L.V.S., Florisbal, L.M., Almeida, B.S., Geraldes, M., 2020b. Dom Feliciano Belt orogenic cycle tracked by its pre-collisional magmatism: the Tonian (ca. 800 Ma) Porto Belo Complex and its correlations in southern Brazil and Uruguay. Precambrian Res 105702. https://doi.org/10.1016/j.precamres.2020.105702

DePaolo, D.J., 1981. A neodymium and strontium isotopic study of the Mesozoic calc-alkaline granitic batholiths of the Sierra Nevada and Peninsular Ranges, California. J Geophys Res Solid Earth 86, 10470–10488. https://doi.org/10.1029/JB086iB11p10470

DePaolo, D.J., Wasserburg, G.J., 1979. Petrogenetic mixing models and Nd-Sr isotopic patterns. Geochim Cosmochim Acta 43, 615–627. https://doi.org/10.1016/0016-7037(79)90169-8

Fernandes, L.A.D., Menegat, R., Costa, A.F.U., Koester, E., Porcher, C.C., Tommasi, A., Kraemer, G., Ramgrab, G.E., Camozzato, E., 1995. Evolução Tectônica Do Cinturão Dom Feliciano No Escudo Sul-Rio-Grandense: Parte Ii - Uma Contribuição a Partir Das Assinaturas Geofísicas. Rev Bras Geociências 25, 375–384. https://doi.org/10.25249/0375-7536.1995375384

Fernandes, L.A.D., Tommazi, A., Porcher, C.C., 1992. Deformation patterns in the southern Brazilian branch of the Dom Feliciano Belt: A reppraisal. J South Am Earth Sci 5, 77–96.

Fernandes, L.A.D.A., Koester, E., 1999. The Neoproterozoic Dorsal de Cangucu strike-slip shear zone: Its nature and role in the tectonic evolution of southern Brazil. J African Earth Sci 29, 3–24. https://doi.org/10.1016/S0899-5362(99)00076-7

Fragoso-Cesar, A.R.S., Figueiredo, M.C.H., Soliani Jr, E., Faccini, U.F., 1986. O Batólito Pelotas (Proterozóico Superior/Eopaleozóico) no escudo do Rio Grande do Sul. XXXIV Congr Bras Geol 1321–1342.

Frimmel, H., Frank, W., 1998. Neoproterozoic tectono-thermal evolution of the Gariep Belt and its basement, Namibia and South Africa. Precambrian Res 90, 1–28. https://doi.org/10.1016/S0301-9268(98)00029-1

Frimmel, H.E., 2018. The Gariep Belt, in: Geology of Southwest Gondwana. pp. 353–386. https://doi.org/10.1007/978-3-319-68920-3_13

Frimmel, H.E., Basei, M.S., Gaucher, C., 2011. Neoproterozoic geodynamic evolution of SW-Gondwana: A southern African perspective, International Journal of Earth Sciences. https://doi.org/10.1007/s00531-010-0571-9

Gollmann, K., Charão Marques, J., José, ;, Frantz, C., Farid, &, Junior, C., 2008. Geoquímica e Isotópos de Nd de Rochas Metavulcânicas da Antiforme Capané, Complexo Metamórfico Porongos, RS. Rev Pesqui em Geociências 35, 83–95.

Goscombe, B., Gray, D., Armstrong, R., Foster, D.A., Vogl, J., 2005. Event geochronology of the Pan-African Kaoko Belt, Namibia. Precambrian Res 140, 103.e1-103.e41. https://doi.org/10.1016/j.precamres.2005.07.003

Goscombe, B., Gray, D.R., 2007. The Coastal Terrane of the Kaoko Belt, Namibia: Outboard arc-terrane and tectonic significance. Precambrian Res 155, 139–158. https://doi.org/10.1016/j.precamres.2007.01.008

Goscombe, B.D., Gray, D.R., 2008. Structure and strain variation at mid-crustal levels in a transpressional orogen: A review of Kaoko Belt structure and the character of West Gondwana amalgamation and dispersal. Gondwana Res 13, 45–85. https://doi.org/10.1016/j.gr.2007.07.002

Gregory, T.R., Bitencourt, M. de F., Nardi, L.V.S., Florisbal, L.M., Chemale, F., 2015. Geochronological data from TTG-type rock associations of the Arroio dos Ratos Complex and implications for crustal evolution of southernmost Brazil in Paleoproterozoic times. J South Am Earth Sci 57, 49–60. https://doi.org/10.1016/j.jsames.2014.11.009

Gross, A.O.M.., Porcher, C.C., Fernandes, L.A.D., Koester, E., 2006. Neoproterozoic low-pressure/high-temperature collisional metamorphic evolution in the Varzea do Capivarita Metamorphic Suite, SE Brazil: Thermobarometric and Sm/Nd evidence. Precambrian Res 147, 41–64. https://doi.org/10.1016/j.precamres.2006.02.001

Gross, A.O.M.S., Droop, G.T.R., Porcher, C.C., Fernandes, L.A.D., 2009. Petrology and thermobarometry of mafic granulites and migmatites from the Chafalote Metamorphic Suite: New insights into the Neoproterozoic P–T evolution of the Uruguayan—Sul-Rio-Grandense shield. Precambrian Res 170, 157–174. https://doi.org/10.1016/j.precamres.2009.01.011

Hartmann, L.A., Leite, J.A.D., Da Silva, L.C., Remus, M.V.D., McNaughton, N.J., Groves, D.I., Fletcher, I.R., Santos, J.O.S., Vasconcellos, M.A.Z., 2000. Advances in SHRIMP geochronology and their impact on understanding the tectonic and metallogenic evolution of southern Brazil. Aust J Earth Sci 47, 829–844. https://doi.org/10.1046/j.1440-0952.2000.00815.x

Hartmann, L.A., Santos, J.O.S., Leite, J.A.D., Porcher, C.C., Mcnaughton, N.J., 2003. Metamorphic evolution and U-Pb zircon SHRIMP geochronology of the Belizário ultramafic amphibolite, Encantadas Complex, southernmost Brazil. An Acad Bras Cienc 75, 393–403. https://doi.org/10.1590/S0001-37652003000300010

Heine, C., Zoethout, J., Müller, R.D., 2013. Kinematics of the South Atlantic rift. Solid Earth 4, 215–253. https://doi.org/10.5194/se-4-215-2013

Höfig, D.F., Marques, J.C., Basei, M.A.S., Giusti, R.O., Kohlrausch, C., Frantz, J.C., 2018. Detrital zircon geochronology (U-Pb LA-ICP-MS) of syn-orogenic basins in SW Gondwana: New insights into the Cryogenian-Ediacaran of Porongos Complex, Dom Feliciano Belt, southern Brazil. Precambrian Res 306, 189–208. https://doi.org/10.1016/j.precamres.2017.12.031

Hueck, M., Oriolo, S., Basei, M.A.S., Oyhantçabal, P., Heller, B.M., Wemmer, K., Siegesmund, S., 2022. Archean to early Neoproterozoic crustal growth of the southern South American Platform and its wide-reaching “African” origins. Precambrian Res 369. https://doi.org/10.1016/j.precamres.2021.106532

Irvine, T.N., Baragar, W.R.A., 1971. A Guide to the Chemical Classification of the Common Volcanic Rocks. Can J Earth Sci 8, 523–548. https://doi.org/10.1139/e71-055

Jost, H., Bitencourt, M.F., 1980. Estratigrafia e tectônica de uma fração da Faixa de Dobramentos Tijucas no Rio Grande do Sul. Acta Geol Leop 11, 27–59.

Knijnik, D.B., 2018. Geocronologia U-Pb e geoquímica isotópica Sr-Nd dos granitoides sintectônicos às zonas de cisalhamento transcorentes Quitéria Serra do Erval e Dorsal de Canguçu, Rio Grande do Sul, Brasil. PhD Thesis. Universidade Federal do Rio Grande do Sul, Porto Alegre - RS. In: http://hdl.handle.net/10183/182067

Koester, E., Porcher, C.C., Pimentel, M.M., Fernandes, L.A.D., Vignol-Lelarge, M.L., Oliveira, L.D., Ramos, R.C., 2016. Further evidence of 777 Ma subduction-related continental arc magmatism in Eastern Dom Feliciano Belt, southern Brazil: The Chácara das Pedras Orthogneiss. J South Am Earth Sci 68, 155–166. https://doi.org/10.1016/j.jsames.2015.12.006

Konopásek, J., Janoušek, V., Oyhantçabal, P., Sláma, J., Ulrich, S., 2018. Did the circum-Rodinia subduction trigger the Neoproterozoic rifting along the Congo–Kalahari Craton margin? Int J Earth Sci 107, 1859–1894. https://doi.org/10.1007/s00531-017-1576-4

Le Bas, M.J., Le Maitre, R.W., Streckeisen, A., Zanettin, B., 1986. A chemical classification of volcanic rocks based on the total alkali silica diagram. J Petrol 27, 745–750. https://doi.org/10.1093/petrology/27.3.745

Leite, J.A.D., Hartman, L.O.A., McNaughton, N.J., Chemale, F., 1998. SHRIMP U/Pb zircon geochronology of neoproterozoic juvenile and crustal-reworked terranes in southernmost brazil. Int Geol Rev 40, 688–705. https://doi.org/10.1080/00206819809465232

Leite, J.A.D., Hartmann, L.A., Fernandes, L.A.D., McNaughton, N.J., Soliani, Jr., Ê., Koester, E., Santos, J.O.S., Vasconcellos, M.A.Z., 2000. Zircon U–Pb SHRIMP dating of gneissic basement of the Dom Feliciano Belt, southernmost Brazil. J South Am Earth Sci 13, 739–750. https://doi.org/10.1016/S0895-9811(00)00058-4

Lena, L.O., Pimentel, M.M., Philipp, R.P., Armstrong, R., Sato, K., 2014. The evolution of the Neoproterozoic São Gabriel juvenile terrane, southern Brazil based on high spatial resolution U-Pb ages and δ18O data from detrital zircons. Precambrian Res 247, 126–138. https://doi.org/10.1016/j.precamres.2014.03.010

Lenz, C., 2006. Evolução metamórfica dos metapelitos da Antiforme Serra dos Pedrosas: condições e idades do metamorfismo p. 111. Master's Thesis. Universidade Federal do Rio Grande do Sul, Porto Alegre, Brasil. In: http://hdl.handle.net/10183/8520

Lenz, C., Fernandes, L.A.D., McNaughton, N.J., Porcher, C.C., Masquelin, H., 2011. U–Pb SHRIMP ages for the Cerro Bori Orthogneisses, Dom Feliciano Belt in Uruguay: Evidences of a ~800Ma magmatic and ~650Ma metamorphic event. Precambrian Res 185, 149–163. https://doi.org/10.1016/j.precamres.2011.01.007

Marques, J.C., Jost, H., Roisenberg, A., Frantz, J.C., 1998. Eventos ígneos da Suíte Metamórfica Porongos na área da Antiforme Capané, Cachoeira do Sul, RS. Rev Bras Geociências 28, 419–430. https://doi.org/10.25249/0375-7536.1998419430

Marques, J.C., Roisenberg, A., Jost, H., Frantz, J.C., Teixeira, R.S., 2003. Geologia e geoquímica das rochas metaultramáficas da antiforme Capané, suíte metamórfica Porongos, RS. Rev Bras Geociências 33, 83–94.

Martil, M.M.D., 2016. O magmatismo de arco continental pré-colisional (790 ma) e a reconstituição espaço-temporal do regime transpressivo (650 ma) no Complexo Várzea Do Capivarita, Sul da Província Mantiqueira. PhD Thesis. Universidade Federal do Rio Grande do Sul, Porto Alegre, Brasil. In: http://hdl.handle.net/10183/149194

Martil, M.M.D., Bitencourt, M. de F., Nardi, L.V.S., 2011. Caracterização estrutural e petrológica do magmatismo pré-colisional do Escudo Sul-rio-grandense: Os ortognaisses do Complexo Metamórfico Várzea do

Capivarita. Pesqui em Geociencias 38, 181–201.

Martil, M.M.D., Bitencourt, M. de F., Nardi, L.V.S., Schmitt, R. da S., Weinberg, R., 2017. Pre-collisional, Tonian (ca. 790 Ma) continental arc magmatism in southern Mantiqueira Province, Brazil: Geochemical and isotopic constraints from the Várzea do Capivarita Complex. Lithos 274–275, 39–52. https://doi.org/10.1016/j.lithos.2016.11.011

Oliveira, C.H.E., Chemale, F., Jelinek, A.R., Bicca, M.M., Philipp, R.P., 2014. U-Pb and Lu-Hf isotopes applied to the evolution of the late to post-orogenic transtensional basins of the dom feliciano belt, Brazil. Precambrian Res 246, 240–255. https://doi.org/10.1016/j.precamres.2014.03.008

Oriolo, S., Oyhantçabal, P., Wemmer, K., Siegesmund, S., 2017. Contemporaneous assembly of Western Gondwana and final Rodinia break-up: Implications for the supercontinent cycle. Geosci Front 8, 1431–1445. https://doi.org/10.1016/j.gsf.2017.01.009

Oyhantçabal, P., Siegesmund, S., Wemmer, K., Presnyakov, S., Layer, P., 2009. Geochronological constraints on the evolution of the southern Dom Feliciano Belt (Uruguay). J Geol Soc London 166, 1075–1084. https://doi.org/10.1144/0016-76492008-122

Padilha, D.F., Bitencourt, M. de F., Nardi, L.V.S., Florisbal, L.M., Reis, C., Geraldes, M., Almeida, B.S., 2019. Sources and settings of Ediacaran post-collisional syenite-monzonite-diorite shoshonitic magmatism from southernmost Brazil. Lithos. https://doi.org/10.1016/j.lithos.2019.06.004

Paim, P.S.G., Chemale Junior, F., Wildner, W., 2014. ESTÁGIOS EVOLUTIVOS DA BACIA DO CAMAQUÃ (RS). Ciência e Nat 36, 183–193. https://doi.org/10.5902/2179460X13748

Pearce, J.A., 1995. Tectonic Implications of Volcanic Arc Magmas. Annu Rev Earth Planet Sci 23, 251–285. https://doi.org/0084-6597/95/0515-0251

Pearce, J.A., Harris, N.B.W., Tindle, A.G., 1984. Trace Element Discrimination Diagrams for the Tectonic Interpretation of Granitic Rocks. J Petrol 25, 956–983. https://doi.org/10.1093/petrology/25.4.956

Peccerillo, A., Taylor, S.R., 1976. Geochemistry of eocene calc-alkaline volcanic rocks from the Kastamonu area, Northern Turkey. Contrib to Mineral Petrol 58, 63–81. https://doi.org/10.1007/BF00384745

Peel, E., Sánchez, L., Angelo, M., Basei, S., 2018. Journal of South American Earth Sciences Geology and geochronology of Paso del Dragón Complex (northeastern Uruguay): Implications on the evolution of the Dom Feliciano Belt (Western Gondwana). J South Am Earth Sci 85, 250–262.

https://doi.org/10.1016/j.jsames.2018.05.009

Percival, J.J., Konopásek, J., Anczkiewicz, R., Ganerød, M., Sláma, J., Campos, R.S., Bitencourt, M. de F., 2022. Tectono-Metamorphic Evolution of the Northern Dom Feliciano Belt Foreland, Santa Catarina, Brazil: Implications for Models of Subduction-Driven Orogenesis. Tectonics 41. https://doi.org/10.1029/2021TC007014

Percival, J.J., Konopásek, J., Eiesland, R., Sláma, J., de Campos, R.S., Battisti, M.A., Bitencourt, M. de F., 2021. Pre-orogenic connection of the foreland domains of the Kaoko–Dom Feliciano–Gariep orogenic system. Precambrian Res 354, 106060. https://doi.org/10.1016/j.precamres.2020.106060

Pertille, J., Hartmann, L.A., Philipp, R.P., Petry, T.S., de Carvalho Lana, C., 2015. Origin of the Ediacaran Porongos Group, Dom Feliciano Belt, southern Brazilian Shield, with emphasis on whole rock and detrital zircon geochemistry and U-Pb, Lu-Hf isotopes. J South Am Earth Sci 64, 69–93. https://doi.org/10.1016/j.jsames.2015.09.001

Pertille, J., Hartmann, L.A., Santos, J.O.S., McNaughton, N.J., Armstrong, R., 2017. Reconstructing the Cryogenian–Ediacaran evolution of the Porongos fold and thrust belt, Southern Brasiliano Orogen, based on Zircon U–Pb–Hf–O isotopes. Int Geol Rev 59, 1532–1560. https://doi.org/10.1080/00206814.2017.1285257

Philipp, R., Machado, R., 2002. O magmatismo granítico Neoproterozóico do Batólito Pelotas no sul do Brasil: novos dados e revisão da geocronologia regional. Rev Bras Geociencias 32, 277–290.

Philipp, R.P., Bom, F.M., Pimentel, M.M., Junges, S.L., Zvirtes, G., 2016a. SHRIMP U-Pb age and high temperature conditions of the collisional metamorphism in the Várzea do Capivarita Complex: Implications for the origin of Pelotas Batholith, Dom Feliciano Belt, southern Brazil. J South Am Earth Sci 66, 196–207. https://doi.org/10.1016/j.jsames.2015.11.008

Philipp, R.P., Lusa, M., Nardi, L.V.S., 2008. Petrology of dioritic, tonalitic and trondhjemitic gneisses from Encantadas Complex, Santana da Boa Vista, southernmost Brazil: paleoproterozoic continental-arc magmatism. An Acad Bras Cienc 80, 735–748. https://doi.org/10.1590/S0001-37652008000400013

Philipp, R.P., Pimentel, M.M., Chemale Jr, F., 2016b. Tectonic evolution of the Dom Feliciano Belt in Southern Brazil: Geological relationships and U-Pb geochronology. Brazilian J Geol 46, 83–104. https://doi.org/10.1590/2317-4889201620150016

Pin, C., Gannoun, A., Dupont, A., 2014. Rapid, simultaneous separation of Sr, Pb, and Nd by extraction chromatography prior to isotope ratios determination by TIMS and MC-ICP-MS. J Anal At Spectrom 29, 1858–1870. https://doi.org/10.1039/C4JA00169A

Ramos, V.A., Cingolani, C., Junior, F.C., Naipauer, M., Rapalini, A., 2017. The Malvinas (Falkland) Islands revisited: The tectonic evolution of southern Gondwana based on U-Pb and Lu-Hf detrital zircon isotopes in the Paleozoic cover. J South Am Earth Sci 76, 320–345. https://doi.org/10.1016/j.jsames.2016.12.013

Rapela, C.W., Fanning, C.M., Casquet, C., Pankhurst, R.J., Spalletti, L., Poiré, D., Baldo, E.G., 2011. The Rio de la Plata craton and the adjoining Pan-African/brasiliano terranes: Their origins and incorporation into south-west Gondwana. Gondwana Res 20, 673–690. https://doi.org/10.1016/j.gr.2011.05.001

Remus, M. V.D., Hartmann, L.A., McNaughton, N.J., Groves, D.I., Fletcher, I.R., 2000. The link between hydrothermal epigenetic copper mineralization and the Cacapava Granite of the Brasiliano cycle in southern Brazil. J South Am Earth Sci 13, 191–216. https://doi.org/10.1016/S0895-9811(00)00017-1

Rivera, C.B., 2016. Construção do maciço sienítico Piquiri (609 a 683 Ma) por colocação sucessiva de pulsos de magma ultrapotássico e shoshonítico sob extensão no Escudo sul-rio-grandense. PhD Thesis. Universidade Federal do Rio Grande do Sul, Porto Alegre, Brasil. In: http://hdl.handle.net/10183/201719

Saalmann, K., Gerdes, A., Lahaye, Y., Hartmann, L.A., Remus, M.V.D., Läufer, A., 2011. Multiple accretion at the eastern margin of the Rio de la Plata craton: the prolonged Brasiliano orogeny in southernmost Brazil. Int J Earth Sci 100, 355–378. https://doi.org/10.1007/s00531-010-0564-8

Saalmann, K., Hartmann, L.A., Remus, & M., 2005. Tectonic Evolution of Two Contrasting Schist Belts in Southernmost Brazil: A Plate Tectonic Model for the Brasiliano Orogeny. Int Geol Rev 4712, 1234–1259. https://doi.org/10.2747/0020-6814.47.12.1234

Saalmann, K., Hartmann, L.A., Remus, M. V.D., 2007. The assembly of West Gondwana—The view from the Rio de la Plata craton, in: Special Paper 423: The Evolution of the Rheic Ocean: From Avalonian-Cadomian Active Margin to Alleghenian-Variscan Collision. Geological Society of America, pp. 1–26. https://doi.org/10.1130/2007.2423(01)

Saalmann, K., Remus, M.V.D., Hartmann, L.A., 2006. Structural evolution and tectonic setting of the Porongos belt, southern Brazil. Geol Mag 143, 59. https://doi.org/10.1017/S0016756805001433

Souza, T.L., 2020. Gênese Dos Serpentinitos E Esteatitos Do Complexo Passo Feio (Rs-Brasil): Evidências

Mineralógicas , Geoquímicas e Isotópicas Gênese Dos Serpentinitos e Esteatitos Do Complexo Passo Feio (RS-Brasil): Evidências Mineralógicas , Geoquímicas E Isotópicas, PhD Thesis. Univesidade Federal do Rio Grande do Sul, Porto Alegre - RS. In: http://hdl.handle.net/10183/221352

Tull, J., Holm-Denoma, C.S., Barineau, C.I., 2014. Early to middle Ordovician back-arc basin in the southern Appalachian Blue Ridge: Characteristics, extent, and tectonic significance. Bull Geol Soc Am 126, 990–1015. https://doi.org/10.1130/B30967.1

Vidal, M., Alric, G., 1994. The palaeoproterozoic (Birimian) of Haute-Comoé in the West African craton, Ivory Coast: a transtensional back-arc basin. Precambrian Res 65, 207–229. https://doi.org/10.1016/0301-9268(94)90106-6

Vieira, D.T., Koester, E., Ramos, R.C., Porcher, C.C., D'Ávila Fernandes, L.A., 2020. SHRIMP U-Pb zircon ages for the synkinematic magmatism in the Dorsal de Canguçu Transcurrent Shear Zone, Dom Feliciano Belt (Brazil): Tectonic implications. J South Am Earth Sci 100, 102603. https://doi.org/10.1016/j.jsames.2020.102603

Werle, M., Hartmann, L.A., Queiroga, G.N., Lana, C., Pertille, J., Michelin, C.R.L., Remus, M.V.D., Roberts, M.P., Castro, M.P., Leandro, C.G., Savian, J.F., 2020. Oceanic crust and mantle evidence for the evolution of Tonian-Cryogenian ophiolites, southern Brasiliano Orogen. Precambrian Res 351, 105979. https://doi.org/10.1016/j.precamres.2020.105979

Whitney, D.L., Evans, B.W., 2010. Abbreviations for names of rock-forming minerals. Am Mineral 95, 185–187. https://doi.org/10.2138/am.2010.3371

Will, T.M., Gaucher, C., Ling, X.-X., Li, X.-H., Li, Q.-L., Frimmel, H.E., 2019. Neoproterozoic magmatic and metamorphic events in the Cuchilla Dionisio Terrane, Uruguay, and possible correlations across the South Atlantic. Precambrian Res 320, 303–322. https://doi.org/10.1016/j.precamres.2018.11.004

Winchester, J.A., Floyd, P.A., 1977. Geochemical discrimination of different magma series and their differentiation products using immobile elements. Chem Geol 20, 325–343. https://doi.org/10.1016/0009-2541(77)90057-2

Zvirtes, G., Philipp, R.P., Camozzato, E., Guadagnin, F., 2017. Análise estrutural do Metagranito Capané, Complexo Porongos, Cachoeira do Sul, RS. Pesqui em Geociências 44, 05. https://doi.org/10.22456/1807-9806.78250

TABLES

Table 1. Comparison of the zircon data among studied samples: their ages, Th/U ratios and isotopic oxygen data (consider only the spots less than 5% discordant).

Coordinate (Zone 22J) Córrego Alegre	**Sample**	**Neoprot. Zircon - n of spots**	**Protolith Age (Ma - 2σ)**	**Th/U Ratio (average)**	**Mean $\delta^{18}O$ (‰ VSMOV)**				**Inherited Zircon**		
					Neoprot. zircon cores		**Neoprot. zircon rims**		**number of spots**	**Age (Ga)**	**Th/U Ratio**
					n		**n**				
341622 m W 6632227 m S	TM-36F	20	786 ± 5 (concordia)	0.28 to 0.68 (0.47)	10	8.41 ± 0.13	6	8.44 ± 0.13	1	Ca. 1.1	0.84
348665 m W 6634440 m S	TM-45G	10	780 ± 10 (Mean ^{206}Pb /^{238}U/)	0.16 to 0.47 (0.33)	2	8.68 ± 0.14	6	8.29 ± 0.33	2	Ca. 1.8 and 2.0 Ga	0.54 and 0.48
326982 m W 6632336 m S	TM-26A	15	787 ± 5 (concordia)	0.26 to 0.67 (0.42)	4	8.75 ± 0.72	13	9.26 ± 0.13	2	Ca. 2.0	0.44 and 0.65
-	-	**Neoprot. Population**	**Provenance Peak (Ma)**	-	-	-	-	-	**Mesoprot. Zircons**	**-**	-
341622 m W 341622 m S	TM-36S	59	750-790	0.18 to 0.70 (0.34)	11	8.03 ± 0.33	2	6.45 ± 1.48	2	Ca. 1.0 and 1.1	0.42 and 0.44

Table 2. Ortho-metamorphic protoliths ages of VCC, PMC and COC.

Complex	Symbology in Fig. 2	Sample	Lithology	U-Pb Zircon (number analyses)			Age (Ma)	Inherited Zircon Age(Ga)	Reference
				SHRIMP	LA-ICP-MS	TIMS			
VCC	1	**TM-36F**	**Tonalitic orthogneiss**	**21**			**785 ± 9**	**Ca. 1.1**	**This paper**
		TM 36 B	Mafic Gneiss	12			782 ± 9.7		(Martil, 2016)
		TM 36 B	Mafic Gneiss		9		790 ± 34		
		TM 36 L	Mafic Gneiss	13			788 ± 5.3		
	2	**TM-45G**	**Granitic orthogneiss**	**11**			**780 ± 10**	**Ca. 1.8 and Ca 2.0**	**This paper**
	3	TM 01 E	Tonalitic orthogneiss		22		791 ± 30	1.6, 1.8 and 3.1	(Martil, 2016)
	4	TM 96 A	Granitic Vein	6			770 ± 9.9	Ca 1.8	
Cerro Olivo Complex		U16-20	Orthogneiss		13 spot SIMS		777 ± 6.1		(Will et al., 2019)
		U16-38	Orthogneiss		12 spot SIMS		782 ± 5.1		
		U16-42	Orthogneiss		21 spot SIMS		783 ± 4.2		
		AC-133-B	Mafic granulite	25			794±8	Ca. 1.2	(Lenz et al., 2011)
		AC296-M	Mafic granulite	18			796±8	Ca. 1.4 and Ca 0.8	
		AC-373-B	Mafic granulite	29			795±8	Ca 0.8	
		PCH-0869	Mafic granulite	36			788±6		
		CH-33-A	Mafic granulite	12			767±9		
		CH-43-D	Mafic granulite	16			772–765?	1.3 and 1.0	
		UY-2-A	Mafic Gneiss	18			771±6	Ca 1.1 to Ca 0.8	
		AC-137-B	Felsic gneiss	20			793±4	Ca 2.1 and Ca 1.2	
		AC-338-A	Felsic gneiss	12			802±12	Ca 1.1	
		CH-174	Felsic gneiss	15			786±9	Ca 1.5 and Ca 0.9	
		COR-42	Felsic mylonite	27			797±8		
		AC-370-A	Felsic migmatite	40			780±5		
		AC-104	Cerro Bori metatonalite	29			779 ± 6	1.3 to 1.0	(Masquelin et al., 2011)
		UCUR-03	Deformed migmatite	15			761 ± 7	Ca 1.1	(Basei et al., 2011)
		UY-10-05	Grt leucocratic gneiss	5			776 ± 12		(Oyhantçabal et al., 2009)
		Sample 1	Migmatite Rocha Syenogranite	10			762 ± 8	Ca. 2.0 and Ca 1.9	(Hartmann et al., 2002)
Eastern-PMC	24	**TM-26A**	**Metarhyolite**	**15**			**788 ± 5**	**Ca. 2.0**	**This paper**
	25	R-088	Metarhyolite	9			773 ± 3	Ca 2.1	(Pertille et al., 2017)
	26	R-015	Metarhyodacite	11			801 ± 4	Ca 1.7	
	27	R-001	Metarhyodacite	14			809 ± 4.1	Ca 2.1 and Ca 1.7	
	28	BR-145	Metarhyolite		29		789 ± 7		(Saalmann et al., 2011)
	29	ESJ-HH7-1D	Metandesite		Rb-Sr Ishocrons		789 ± 39		(Soliani Jr, 1986)
		ESJ-HH7-1E	Metandesite		Rb-Sr Ishocrons		949 ± 45		
		ESJ-HH7-2C	Metandesite		Rb-Sr Ishocrons		1542 ± 83		
	30		Metaandesite			x	773 ± 8		(Chemale, 2000)
Western -PMC	31	CA-16	Metavolcano-sedimentary rock		24		615 ± 3.4		(Höfig et al., 2018)
	32	CA-11	Metavolcano-sedimentary rock		15		600 ± 7		
	33		Deformed alkaline gneiss		x		603 ± 6		(Zvirtes et al., 2017)
			Deformed alkaline gneiss			x	543 ± 5		(Chemale, 2000)
	34	CP3	Rodingite blackwall (Capané ophiolite)		131		793±1 to 715±2		(Arena et al., 2018)

Table 3. Provenances sources ages of VCC, PMC and COC

Complex	Symbology in Fig. 2	Sample	Lithology	U-Pb Zircon (number of analyses)		Provenance interval (Ma)	Provenance Peak (Ma)	Provenance Younger than 640 Ma (N of grains)	Reference
				SHRIMP	LA-ICP-MS				
VCC	1	**TM-36S**	**paragnaisse**	**45**		**716 - 1091**	**750-790**	**No**	**This paper**
	2	SMVC80	Metapelitic Gneisse	32				No	
	3	SMVCA	Metapelitic Gneisse		20	728 - 2497	2107.9 ± 2.4	No	
		SMVCB	Metapelitic Gneisse		64			No	
	2	13-Mar							(Gruber et al., 2016a)
		VC12-03	Marble	Whole-rock 87Sr/86S		715 - 750		Not aplicable	
	3	PO 21							
		VC 13-1							
COC		UA-37	Quartzite		122	650* - 2800	1450, 1750 and 2000	No	(Konopásek et al., 2018)
		UB-18	Quartzite		112	1100 - 3100	1750 and 2005	No	
Eastern Porongos Metamorphic Complex	4	P-122	quartzite	36		994 ± 5 - 2,705±17	1306	No	(Pertille et al., 2017)
	5	T-148	plg-qtz-chl-ms schist	28		605±5 - 2,937 ± 8	2171	Yes (2)**	
	6	PJP-06	ms schist		61	1008±12 - 2863±24	1187	No	(Pertille et al., 2015a)
	7	POR-18	Metarenite		9	765±19 - 796±19		No	(Gruber et al., 2016b)
	8	RIP-08	qtz mylonite		19	1,750±18 - 2,910±24	2045	No	(Gruber et al., 2011)
	9	POR-04A	chl-ms schist		39	1,010±17 - 2,520±51	2254	No	
	10	POR-12A	qtz-ms schist		22	1,149±26 - 2,652±32	1217	No	
	11	POR-13A	chl-ms schist		11	1,113±42 - 2,195±31	1488	No	
	12	POR-06A	chl-ms schist		2	1,262±31 - 2,093±61		No	
	13	RIP-06	chl-ms schist		15	1,041±46 - 2,220±28		No	
	14	RIP-03	chl-ms schist		11	1,164±21 - 2,414±31	2175	No	
	15	RIP-05	chl-ms schist		11	1,153±20 - 2,169±15		Yes (1)**	
	16	RIP-11	qtz mylonite		48	1,619±39 - 2,906±42	2039	Yes (1)**	
	17	BRAF34	sericitic phyllite	23		620 - 2,200		Yes (1)**	(Basei et al., 2008)
Basement Cover	18	Sample 3	Godinho quartzite		98	1766±40 - 3384±24	2082	No	(Pertille et al., 2015a)
	18	3 - Godinho	quartzite	31		1,990±15 - 2,488±12	2079±14	No	Hartmann et al. (2004)
	19	6 - Jaíba	quartzite	43		1,998±15 - 2,454±12	2070	No	
	20	5 - Figueiras	quartzite	7		2,004±13 - 2,486±20	2100	No	
	21	1 - Alto Bonito	quartzite	21		2,030±21 - 2,459±22	2096	No	
	22	2 - Aberto dos Cerros	quartzite	34		2,015±15 - 3,092±19	2082	No	
	23	4 - Coxilha do Raio	quartzite	31		1,950±78 - 2,449±28	2056±14	No	
		Sample 4	Coxilha do Raio quartzite		96	1980±34 - 2506±38	2074	No	(Pertille et al., 2015a)
Western Porongos Metamorphic Complex	***	CA-11	metavolcano-sedimentary rock		20	584±9 – 2252±34	600	Yes (>10)	(Höfig et al., 2018)
	***	CA-16	metavolcano-sedimentary rock		76	599±5 – 2273±25	615	Yes (>10)	
	24	198	qtz-ms schist	30		579±20 - 2267±14	585 and 2266	Yes (4)	(Pertille et al., 2015b)
		300	alb-chl schist	66		553±6 - 2249±15	619	Yes (>10)	
	25	C-275	metagreywake	33		569±8 - 2,231±16	606	Yes (>10)	(Pertille et al., 2017)
		C-025	metapelite	29		550±10 - 2,811±12	585	Yes (>10)	
	26	C-175	qtz-ms schist	34		751±18 - 2,917±10	2196	No	
	27	CA-02A	phyllonite		56	1890 - 3260	2130	No	(Höfig et al., 2018)
	28	CA-17	qtz mylonite		83	1300 - 2800	2290	No	
	29	CA-21B	qtz-ms ultramyloite		59	2040 - 2860	2170	No	
	30	CA-22	str-grt schist		81	820 – 2250	2120	No	
	31	CA-19	qtz-ms schist		95	572±7 - 1971±27	610 and 770	Yes (>10)	
	32	C-041	gr-bt-ms schist	42		576±8 - 3,156±7	2186	Yes (5)	(Pertille et al., 2017)
	33	C-040	quartzite	36		618±15 - 2,481±30	2.105	Yes (1)**	

*Interpreted as recrystallization of the detrital grains during high-grade metamorphism.

** In spite of the fact that some grains are younger than 640 Ma, such data do not have any statistical meaning. Ca. 640 Ma was set as an age limit for the Neoproterozoic detrital zircon population, as this is the timing of the main metamorphic–deformational phase recorded in the hinterland of DFB (VCC and COC). The best metamorphic age for PMC is a Rb–Sr isochron in muscovite and whole-rock - 658 ± 26 Ma (Lenz, 2006).

*** The location of these samples is provided in table 2.